INVESTIGATION OF TECHNIQUES AND PROCEDURES TO OBTAIN α-Al_2O_3 SCALES ON COATINGS WITH IMPROVED OXIDATION RESISTANCE

by

Erika Meier Jackson

BS, University of Pittsburgh, 2005

Submitted to the Graduate Faculty of

The School of Engineering in partial fulfillment

of the requirements for the degree of

Master of Science

University of Pittsburgh

2007

UNIVERSITY OF PITTSBURGH

SCHOOL OF ENGINEERING

This thesis was presented

by

Erika Meier Jackson

It was defended on

May 21, 2007

and approved by

John P. Leonard, Assistant Professor, Department of Mechanical Engineering and Materials Science

Ian Nettleship, Associate Professor, Department of Mechanical Engineering and Materials Science

Frederick S. Pettit, Professor Emeritus, Department of Mechanical Engineering and Materials Science
Thesis Advisor

INVESTIGATION OF TECHNIQUES AND PROCEDURES TO OBTAIN α-Al_2O_3 SCALES ON COATINGS WITH IMPROVED OXIDATION RESISTANCE

Erika Meier Jackson, MS

University of Pittsburgh, 2007

In this study, two types of coating systems were investigated for their ability to withstand cyclic oxidation conditions. NiCoCrAlY coatings with either 0.1 or 0.5 weight percent yttrium as well as platinum modified aluminide coatings were examined. All of the samples were exposed cyclically, in a bottom-loading furnace at 1100°C in laboratory air. Optical and scanning electron microscopy (SEM) were used to characterize the samples. Various surface treatments were performed on the coatings prior to their exposure. Samples were either exposed as-received, with no treatment, light grit blasted (LGB), light grit blasted and etched with NaOH, or fine polished.

The samples containing 0.5 wt.% Y in the as received, LGB and LGB and etched condition, failed by the formation of large oxide protrusions caused by the preferential oxidation of yttrium and by cracking in the coating. The fine polished NiCoCrAlY coatings containing 0.5 wt.%Y did not develop protrusions and did not fail in test. None of the 0.1 wt.%Y coatings with any treatment developed protrusions and none of these failed in test. The PtAl coatings all failed by the formation of large voids at the coating/substrate interface that coalesced and broke through the coating surface, regardless of surface treatment.

It was concluded that, in the NiCoCrAlY system, the roughness of the coating surface as well as the amount of yttrium present to oxidize in the coating plays a large role in the coating lifetime. In the PtAl coatings, surface preparation did not appear to have an effect on the

coating lifetime. The PtAl coatings and the rough NiCoCrAlY coatings containing 0.5 wt.%Y were found to have similar lifetimes of a few thousand cycles. The polished 0.5 wt.%Y NiCoCrAlY coating and all of the 0.1 wt.%Y coatings exhibited exceptionally long lifetimes, with none of them failing in test.

TABLE OF CONTENTS

ACKNOWLEDGMENTS XII

1.0 INTRODUCTION 1

2.0 BACKGROUND 3

2.1 THERMODYNAMICS OF OXIDATION 3

2.1.1 Selective Oxidation 4

2.2 COATINGS 7

2.2.1 α-Al_2O_3 Formers 8

2.2.2 Aluminide Diffusion Coatings 10

2.2.3 Overlay Coatings 13

2.2.4 Reactive Element Effect 18

2.2.5 Surface Preparation Effects 22

2.3 COATING DEGRADATION AND FAILURE 24

3.0 RESEARCH OBJECTIVES 26

4.0 EXPERIMENTAL PROCEDURE 27

5.0 RESULTS AND DISCUSSION 32

5.1 CYCLIC OXIDATION RESULTS 32

5.1.1 Cyclic Oxidation of NiCoCrAlY Coatings 32

5.1.2 Cyclic Oxidation of Platinum Aluminide Coatings 68

5.1.3 Comparison of Coatings for Cyclic Oxidation Resistance 76

5.1.4 Future Work 77

6.0 CONCLUSIONS 78

BIBLIOGRAPHY 80

LIST OF TABLES

Table 1. Alloy and Coating Composition (Weight %) 27

LIST OF FIGURES

Figure 1. Ellingham Diagram of Selected Oxides [4]..... 5

Figure 2. Al_2O_3- Y_2O_3 Phase Diagram [6]..... 9

Figure 3. Schematic of Pack Cementation Process [9]..... 12

Figure 4. Ni-Al Phase Diagram [4]..... 12

Figure 5. Schematic of Electron Beam-Physical Vapor Deposition Apparatus [4]..... 15

Figure 6. Schematic of Plasma Spray Apparatus [4]..... 17

Figure 7. Cyclic oxidation kinetics for model Ni-Cr-Al alloys exposed at 1100°C [16]..... 18

Figure 8. As-Received NiCoCrAlY Coating..... 29

Figure 9. Hand Polished NiCoCrAlY Coating..... 29

Figure 10. Light Grit Blasted NiCoCrAlY Coating..... 30

Figure 11. Light Grit Blasted & NaOH Etched NiCoCrAlY Coating..... 30

Figure 12. Bottom-Loading Furnace for Cyclic Oxidation Tests..... 31

Figure 13. As-Received NiCoCrAlY Coating Containing 0.1 wt. % Y..... 33

Figure 14. As-Received NiCoCrAlY Coating Containing 0.5 wt. % Y..... 33

Figure 15. As-Received NiCoCrAlY Coating Containing 0.1 wt.% Y at High Magnification... 34

Figure 16. 0.1 wt% Y, LGB Sample after 2000 Cycles..... 35

Figure 17. 0.5 wt% Y, LGB Sample after 2000 Cycles..... 36

Figure 18. Protrusion in 0.5 wt.%, LGB NiCoCrAlY Coating after 2000 Cycles..... 36

Figure 19. Protrusion Extending through Coating into Substrate..... 37

Figure 20. Protrusion Penetrating Original Interface..... 38

Figure 21. Surface Images of Sample Surfaces after 2800 Cycles..... 39

Figure 22. Comparison of 0.5 and 0.1 wt.% Y Coatings after 2800 Cycles..... 39

Figure 23. Comparison of Surface Treatments in 0.5 wt.%Y Coatings after 2800 Cycles..... 41

Figure 24. 0.5 wt.%Y Coatings with Different Treatments after 2800 Cycles..... 41

Figure 25. Surface Images of Sample Surfaces after 3700 Cycles..... 42

Figure 26. Cross section of LGB 0.5 wt.% Y Sample after 3700 Cycles..... 43

Figure 27. Protrusion in 0.5 wt% Y Coating after 3700 Cycles..... 43

Figure 28. Yttrium rich Particles in Protrusion..... 44

Figure 29. High-Magnification Image of Protrusion..... 44

Figure 30. 0.5 wt.% Y, As-Received Coating after 3700 Cycles..... 46

Figure 31. Yttrium rich Particles Incorporated into Oxide in Protrusion..... 46

Figure 32. Spinel at Surface of Protrusion..... 47

Figure 33. 0.5 wt.% Y, Hand Polished after 3700 Cycles at 1100°C..... 49

Figure 34. Small Protrusion in 0.5 wt.% Y, Hand Polished Coating after 3700 Cycles..... 49

Figure 35. 0.1 wt.% Y, Hand Polished after 3700 Cycles at 1100°C..... 50

Figure 36. Hand Polished 0.1 wt.%Y Sample in Figure 35 Etched to Show β-Phase..... 50

Figure 37. Hand Polished Coating with 0.1 wt.% Y after 5000 Cycles..... 52

Figure 38. High Magnification of HP Coating with 0.1 wt.% Y after 5000 Cycles..... 52

Figure 39. As-Received Coating with 0.1 wt.% Y after 6500 Cycles..... 53

Figure 40. TGO on As-Received Sample after 6500 Cycles..... 53

Figure 41. Protrusion Formation in NiCoCrAlY Coatings with Rough Surfaces 55

Figure 42. Advanced Protrusion Formation..... 55

Figure 43. Surface of 0.1 wt.% Y NiCoCrAlY Coating after 100 Cycles at 1100°C..... 58

Figure 44. Surface of 0.5 wt.% Y NiCoCrAlY Coating after 100 Cycles at 1100°C..... 58

Figure 45. Cross-section of As-Received Coating Containing 0.5 wt.% Y after 100 cycles 59

Figure 46. Oxide-filled Protrusion in As-Received Coating 60

Figure 47. Yttrium Particles in As-Received Coating 60

Figure 48. 0.5 wt.% Y, LGB Coating after 300 Cycles..... 62

Figure 49. Protrusion in Coating after 300 Cycles 62

Figure 50. 0.1 wt.% Y, As-Received Coating after 400 Cycles 63

Figure 51. LGB Sample with 0.1 wt.% Y after 1000 Cycles..... 65

Figure 52. Small Protrusion in 0.1 wt.% Y, LGB Sample after 1000 Cycles..... 65

Figure 53. LGB Sample with 0.5 wt.% Y after 1000 Cycles..... 66

Figure 54. Protrusion in 0.5 wt.% Y Sample after 1000 Cycles..... 66

Figure 55. Protrusion and Grain Boundaries in Coating after 1000 Cycles 67

Figure 56. Weight Change vs. Time Plot for PtAl Cyclic Oxidation 69

Figure 57. Cross-section of As-Received PtAl Coating 69

Figure 58. LGB PtAl Coating after 1000 Cycles at 1100°C..... 70

Figure 59. Irregular Surface of PtAl after 1000 Cycles..... 70

Figure 60. Void Formation in PtAl Coating after 1000 Cycles 71

Figure 61. LGB & Etched PtAl Coating after 2300 Cycles at 1100°C 71

Figure 62. LGB & Etched PtAl Coating after 2850 Cycles at 1100°C 73

Figure 63. PtAl Coating Degradation after 2850 Cycles..... 73

Figure 64. LGB and Etched PtAl Coating after 4500 Cycles at 1100°C 74

Figure 65. Voids at Coating/Substrate Interface after 4500 Cycles..... 74

Figure 66. Failure of PtAl Coating after 4500 Cycles 75

ACKNOWLEDGMENTS

First, I must thank Prof. Pettit and my father for their insight, support and encouragement throughout this process. Without their guidance and expertise, none of this would have been possible. I feel very lucky to have been given this opportunity.

I must also thank my committee members, Prof. Leonard and Prof. Nettleship for their participation, both in this process, and in my studies.

My thanks to Scot Laney, Kivilcim Hance, Kee Young Jung, Monica Maris-Jakubowski, and Meltem Yanar for their knowledge and friendship. They made my time here more enjoyable and were never too busy to help with any problem. Al Stewart also deserves many thanks for his endless patience and technical support.

I would like to acknowledge that the financial support that made this program possible came from the Office of Naval Research.

Sincere thanks to my parents, who loved and supported me through many years and several majors. Thanks to my dad for always pushing me to try a little bit harder even when it meant taking the long road, and to my mom for walking with me when that road was a lot bumpier than expected.

Finally, I would like to thank my husband, and best friend, for his loving support and for always telling me I could do it, even when I was convinced I couldn't.

1.0 INTRODUCTION

A major concern in the operation of gas turbine components is the necessity to find materials that will resist high temperature degradation. Generally alumina-forming coatings are put in these roles due to their superior protection. These systems typically consist of a nickel-based superalloy coated with an aluminum-rich MCrAlY bond coat (BC), where M=Ni, Co or both, that is deposited by either plasma spraying or electron beam physical vapor deposition (EBPVD), or a nickel platinum aluminide (PtAl) formed by diffusion processes. At high temperatures, the coating will develop a thermally grown oxide (TGO) that protects the coating from excessive oxidation. Frequently a yittria-stabilized zirconia (YSZ) thermal barrier coating (TBC) is deposited onto the bond coat. During the TBC deposition process, a TGO forms on the bond coat. This oxide layer ideally consists of α-alumina and acts both to bond the TBC to the bond coat and to limit further oxidation in the coating and superalloy. In many applications, TBC's are not necessary, as the bond coat provides excellent protection on its own.

New focus is being placed on ways to extend the life of MCrAlY and PtAl bond coats by improving the properties of the TGO. In the case of TBC coatings, it is frequently found that failure occurs by spalling of the TBC from the BC during cyclic conditions. Being able to precisely control the TGO would significantly enhance the lifetimes of TBC and BC systems. Altering parameters of the BC, such as surface condition and composition, could result in an improved BC/TGO interface.

The effects of the surface condition of NiCoCrAlY bond coats with 0.5 wt% yttrium have been examined [1]. This system was also deposited with a TBC and cyclic lifetimes were studied. Various results were observed based on the different modifications, such as heavy grit-blasting etc., to the bond coats. It is believed that the surface treatments that produced the best results, such as fine polishing, did so by eliminating defects near the TGO surface which are suspected of causing failure. It has been suggested that in NiCoCrAlY bond coats containing 0.3 wt% Y separations between the layers of the system nucleate around imperfections in the TGO [2].

More attention is also being paid to the effect of yttrium additions on coating lives. Yttrium is added to NiCoCrAlY coatings to produce a reactive element effect, discussed in more detail later. While Y has been shown to improve the alumina scale adhesion, oxidized Y_2O_3 can provide a rapid path for oxygen to diffuse into the coating, accelerating degradation. New studies show that in coatings with a rough surface, the yttrium will segregate to concave areas, leaving the convex regions depleted of yttrium [3]. The study also showed that the distribution of yttrium was much more uniform in specimens with a flat surface.

Understanding the effects of Y concentration on NiCoCrAlY's and the effects of surface preparation on NiCoCrAlY and PtAl coatings is an important step in significantly increasing their lifetimes.

2.0 BACKGROUND

2.1 THERMODYNAMICS OF OXIDATION

Predicting if a given material will oxidize, requires a thorough knowledge of the thermodynamics involved in the oxidation reactions. The second law of thermodynamics can be used to determine whether or not a chemical reaction can occur. The Gibbs Free Energy change for a reaction may be expressed as:

$$\Delta G' = \Delta H' - T\Delta S', \qquad \text{(a)}$$

where ΔG′ represents the change in the Gibbs free energy of a system for a given reaction, ΔH′ represents the change in enthalpy and ΔS′ the entropy change. In order for a reaction to proceed, the second law of thermodynamics states that ΔG′ must be less than zero at constant temperature and pressure. If ΔG′=0, the system is said to be in equilibrium, and a ΔG′ greater than zero indicates a reaction that is thermodynamically impossible.

For a given reaction, Equation (b),

$$aA + bB = cC + dD, \qquad \text{(b)}$$

ΔG′ can be calculated using Equation (c),

$$\Delta G' = \Delta G^{\circ} + RT \ln\left(\frac{a_C^c a_D^d}{a_A^a a_B^b}\right), \qquad \text{(c)}$$

where ΔG° represents the change in free energy for components in their standard states and *a* is known as the thermodynamic activity.

ΔG° can be calculated for the reaction shown previously using Equation (d),

$$\Delta G^\circ = c\Delta G_C^\circ + d\Delta G_D^\circ - a\Delta G_A^\circ - b\Delta G_B^\circ, \quad \text{(d)}$$

where ΔG°_B, for example, is the standard molar free energy of formation for species B. These values can be found tabulated in a number of references.

2.1.1 Selective Oxidation

In high temperature oxidation of alloys, it is often necessary to determine which oxide is likely to form under various conditions. Materials used for high temperature applications are generally alumina or chromia formers. Adding sufficient Al or Cr to an alloy will result in selective oxidation, in which case Al or Cr, having a higher affinity for oxygen than other elements in the alloy, will oxidize selectively, forming a protective scale that prevents further oxidation of the alloy. The easiest way to determine which oxide is stable at a given temperature and pressure is to consult an Ellingham Diagram, Figure 1, in which the standard free energy of formation for various compounds is plotted versus temperature. The diagram shown above is for various oxides. The lower the line for a particular oxide is on the diagram, the more stable is that compound. For example, the line representing the formation of Al_2O_3 is significantly lower than the line for NiO. This means that, in an alloy containing Al and Ni, with sufficient Al concentration, the Al would be selectively oxidized, thus forming a protective Al_2O_3 surface layer.

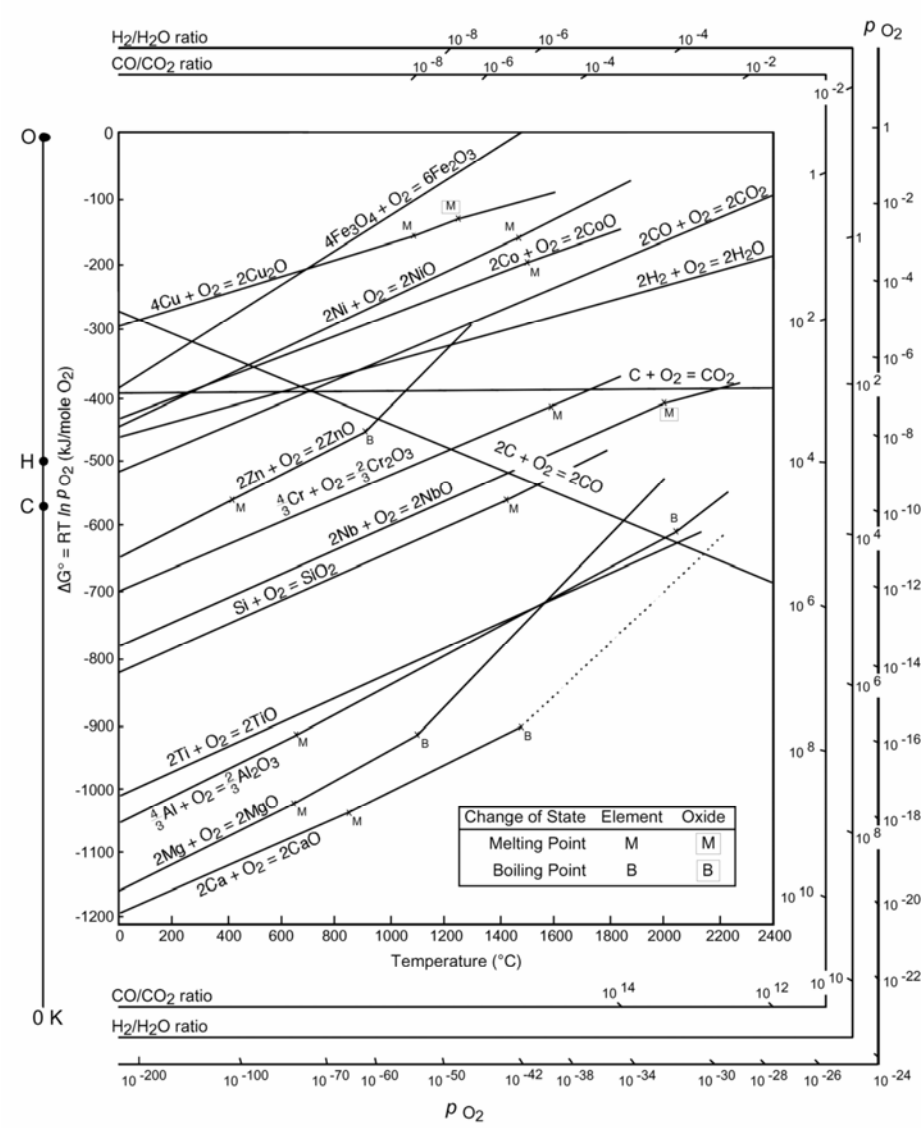

Figure 1. Ellingham Diagram of Selected Oxides [4].

This principle of selective oxidation is the basis for most of the alloys and coatings used in high temperature applications. These alloys generally consist of a base metal composed of Ni, Fe or Co which forms a fairly stable oxide and the alloying element that is usually Al, Cr or Si, which all form very stable oxides [4].

The transition from internal to external oxidation is the basis for the principle of selective oxidation. In internal oxidation, oxygen diffusing into an alloy causes the oxidation of alloying elements below the surface of the material. In high temperature applications this causes problems when elements necessary to form a protective external oxide layer are internally oxidized, depleting the material available for external oxidation. Conditions necessary for internal oxidation are as follows [4]:

1.) The ΔG° of formation of the solute metal oxide must be more negative than the ΔG° of formation of the base metal oxide.

2.) The value of ΔG for the reaction of the oxidation of the solute metal must be negative. This means that the base metal must have a sufficient oxygen solubility to provide the necessary dissolved oxygen activity at the point of the reaction.

3.) The concentration of solute in the alloy must be less than the amount necessary for the transition to external oxidation.

4.) The dissolution of oxygen into the alloy must not be hindered by a surface layer when oxidation begins.

At a certain concentration of a solute metal that is less noble than the base metal, there will be a transition from internal to external oxidation in the alloy and a protective layer of the

solute metal oxide will form on the surface. The penetration velocity of the internal oxidation zone can be calculated using Equation (e) [4].

$$\nu = \frac{N_O^{(S)} D_O}{\nu N_B^{(O)}} \frac{1}{X} \quad \text{(e)}$$

where $N_O^{(S)}$ is the oxygen solubility of the nobler element (A) in a binary alloy. D_O is the diffusivity of oxygen in this element, and $N_B^{(O)}$ is the initial solute (B) concentration. This equation illustrates that either a decrease in the oxygen solubility of A, or increasing the initial solute concentration, decreases the penetration velocity. This means that at a certain concentration of B, the outward diffusion of this element will be rapid enough to produce a continuous surface layer of BO_v that will prevent internal oxidation [4].

2.2 COATINGS

Coatings have been utilized in the protection of materials for hundreds of years. With the increasing demands that modern technology is placing on materials, coatings are finding more and more uses. In the field of high temperature oxidation, coatings are generally employed for two purposes. They are used to protect materials, such as superalloys, that have been designed for properties such as strength, but do not have the ability to withstand high temperature environments. A second use is to protect substrates that are inexpensive, but degrade easily at high temperatures. To provide oxidation resistance, the coatings usually contain elements such as aluminum, chromium or silicon that can form a protective oxide. For the temperatures experienced in gas turbine systems, alumina-formers are, by far, the most protective.

2.2.1 α-Al_2O_3 Formers

The oxidation resistance of bond coats can generally be attributed to the selective oxidation of aluminum in the coating to form a slow growing, continuous alumina scale on the surface of the coating. This alumina scale is known as a thermally grown oxide (TGO) and its properties are very important to the life of the coating. For the maximum protective effect, it is desirable to have a pure α-Al_2O_3 scale, although this is not always possible. Also known as corundum, α-Al_2O_3 is the thermodynamically stable form of alumina, which has a rhombohedral structure. In this structure, the Al cations occupy two thirds of the available octahedral sites between a hexagonal lattice of oxygen anions. Several metastable forms of alumina also exist and commonly form prior to the development of α-Al_2O_3. The cubic spinel form is known as γ-Al_2O_3, a tetragonal form is called δ- Al_2O_3, and the monoclinic form is known as θ- Al_2O_3.

Alpha Al_2O_3 is known to primarily form by the inward migration of oxygen ions along oxide grain boundaries, while the metastable forms of alumina generally form by the outward migration of aluminum cations. The growth of alumina scale follows Wagner's parabolic rate law, but generally slows significantly after continued exposure. This may occur due to a decrease in the number of grain boundaries as they have been found to play an important role in the diffusion of oxygen [5].

Yttrium is frequently added to the system to improve the adherence of the alumina scale. When the Y oxidizes in the presence of the Al_2O_3, as in the case of NiCoCrAlY's, several compounds can form between the Al_2O_3 and the Y_2O_3. The phase diagram for this system is pictured in Figure 2.

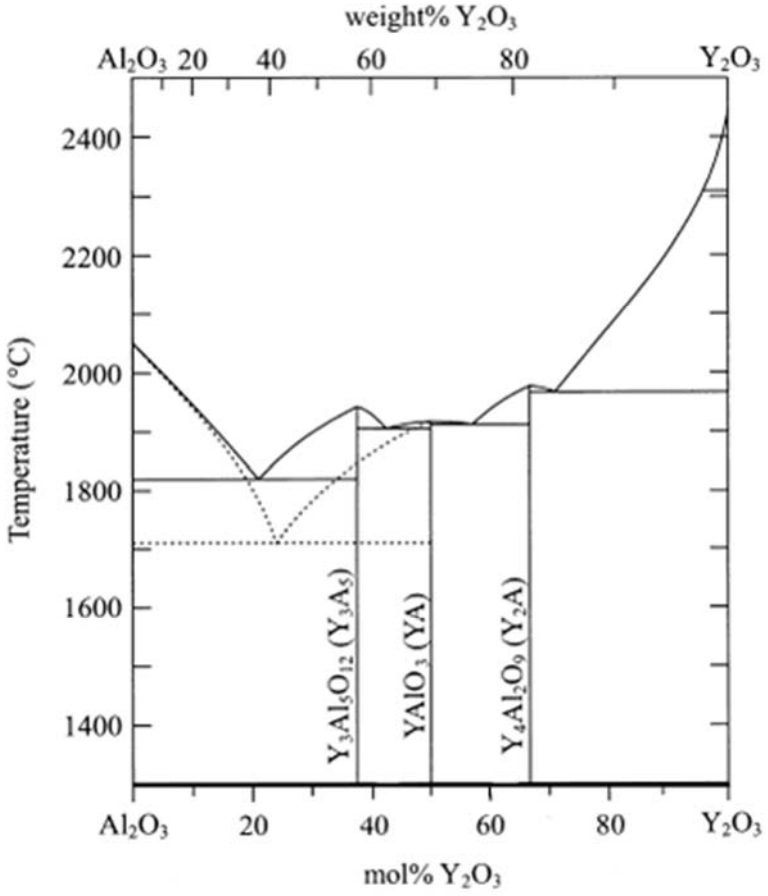

Figure 2. Al_2O_3- Y_2O_3 Phase Diagram [6].

At elevated temperatures, it can be observed from the diagram that the system can form three intermediate phases. The $Y_3Al_5O_{12}$ phase is known as yttrium alumina garnet (YAG). The $YAlO_3$ phase is known as yttria alumina perovskite (YAP) and the $Y_4Al_2O_9$ phase is known as yttria alumina monoclinic (YAM). Several studies have been performed on YAG and it has been found to be compatible with α-alumina due to their similar coefficients of thermal expansion and high melting temperatures [7]. YAG is much less protective than Al_2O_3 due to the higher diffusivity of oxygen in YAG. There is little information on the diffusivity of various components in YAG, but by extrapolation, a diffusivity of approximately 3.16×10^{-15} cm^2/sec can be obtained for bulk diffusion of oxygen in YAG at 1100ºC. This compares to the much slower diffusivity of approximately 1×10^{-20} cm^2/sec for the bulk diffusion of oxygen in Al_2O_3 at the same temperature [8].

2.2.2 Aluminide Diffusion Coatings

The two main types of coatings are diffusion and overlay coatings. Diffusion coatings are made by adding elements that can provide high temperature corrosion resistance to the substrate, such as Al, Cr or Si. The focus of this section will be aluminide diffusion coatings. In diffusion coatings, the coating is composed of materials from the substrate as well as the added material and an interdiffusion zone can be observed in the specimen.

Several methods exist for aluminizing a substrate. Two that will be discussed are Pack cementation and high temperature, low activity chemical vapor deposition (CVD). The pack cementation process is a form of chemical vapor deposition in which a substrate is buried in a powder mixture consisting of the elements to be deposited, a halide salt activator and an inert

filler, generally Al_2O_3. This set-up is shown in Figure 3. The filler is used to provide a diffusion pathway for gases generated during the reaction and to support the components being coated. The heat-resistant container that the mixture is in is sealed and heated to between 700 and 900°C for Al. At these high temperatures, the alloy powder reacts with the halide salt and forms volatile metal halides that travel through the gas generated in the pack. These halides then deposit aluminum which diffuses into, the component [10]. In Ni-based superalloys, the high-activity aluminizing process results in a Ni_2Al_3 matrix with numerous other elements dissolved in solution. The growth-limiting step is the diffusion of the Al through the Ni_2Al_3. An interdiffusion treatment is used to transform the Ni_2Al_3 in to β-NiAl, an Al rich phase. The phase diagram for this system is shown in Figure 4.

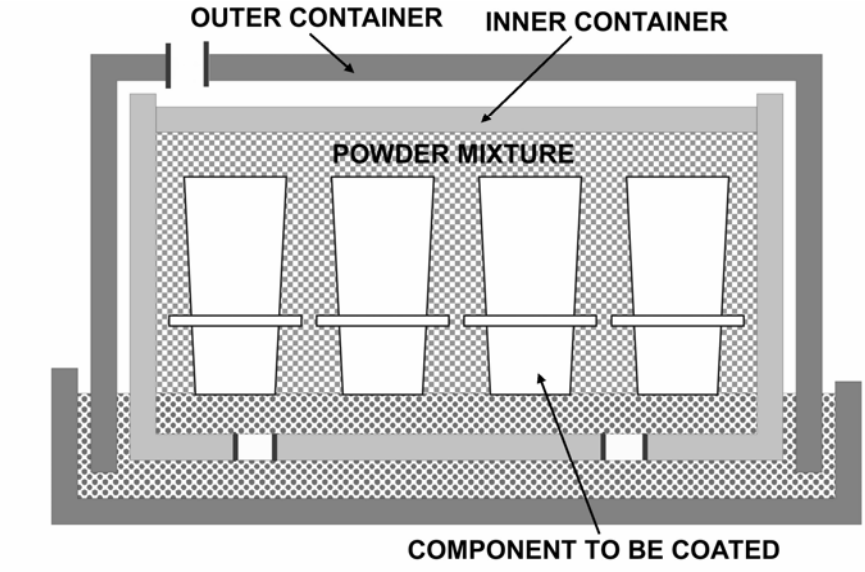

Figure 3. Schematic of Pack Cementation Process [9].

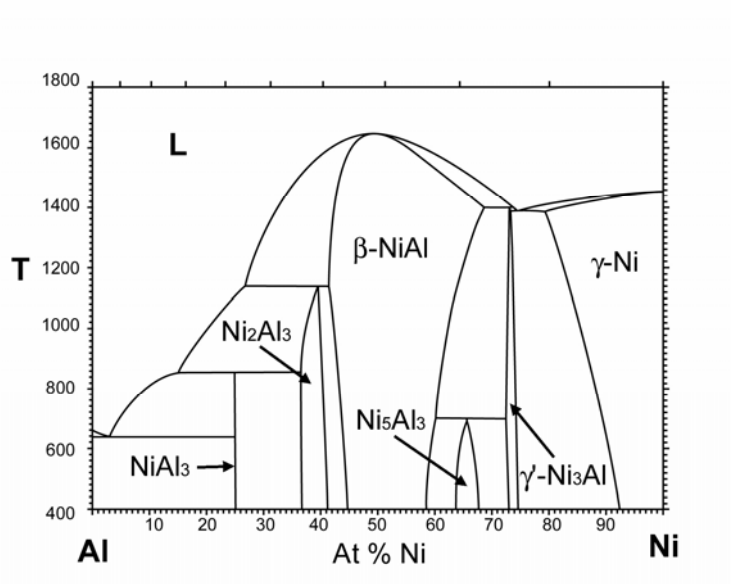

Figure 4. Ni-Al Phase Diagram [4].

The activity of the Al in the pack will ultimately determine which phases will form.

In low activity chemical vapor deposition methods, coating gases that are externally generated are fed into a vacuum chamber containing the substrates to be coated. This allows greater compositional freedom and also allows internal passages in parts, such as turbine blades, to be successfully coated.

After the aluminizing process is complete, upon oxidation, the coating will form a protective alumina layer. Due to the large reservoir of Al that was diffused into the coating, the protective scale can be regenerated after events such as spalling, and should significantly increase the life of the coating. Platinum-modified aluminide coatings have shown even better results than straight aluminides. In these coatings, a thin layer of Pt (5-7μm) is electroplated onto the substrate and given an annealing treatment before the aluminizing process. During aluminizing, the aluminum diffuses through the platinum layer resulting in a β-NiAl structure with the platinum in solution. The platinum additions in these coatings were originally intended to limit the diffusion of aluminum into the substrate, but they have also been found to increase scale adherence, improving cyclic oxidation resistance [11].

2.2.3 Overlay Coatings

Overlay coatings are deposited onto the surface of a substrate and have much less interaction with that substrate than do diffusion coatings. The goal in the deposition of the overlay coating is simply to bond the coating to the substrate, not to cause substantial interdiffusion. This provides a wider range of composition options than are available in diffusion coatings. Reactive

elements, such as Y and elements such as Cr that are almost impossible to incorporate into diffusion coatings can be deposited into overlay coatings [4]. Reactive elements will be discussed in detail in the next subsection. This is very important for the case of MCrAlY coatings, where it has been observed that Cr allows the coating to remain an Al_2O_3 former for Al contents below where this would normally be possible [12].

Overlay coatings are usually deposited by either electron beam-physical vapor deposition (EB-PVD) or spraying methods such as plasma spraying. EB-PVD is frequently used to apply MCrAlY coatings to turbine blades. The process is carried out in a high-vacuum chamber where a high energy electron beam is used to locally melt a section of an MCrAlY target. This produces a vapor containing the components of the coating that deposit onto the substrate which is being rotated above the vapor source. The substrate is generally preheated to improve adherence of the coating. A schematic of the process in shown in Figure 5.

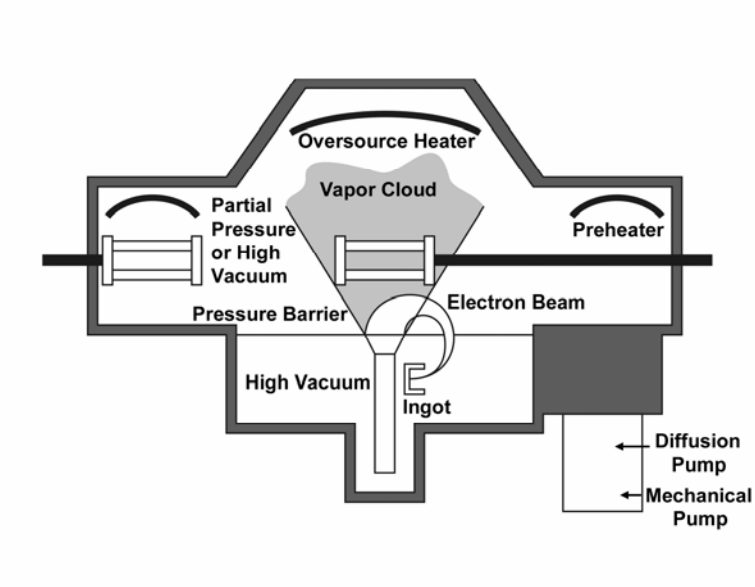

Figure 5. Schematic of Electron Beam-Physical Vapor Deposition Apparatus [4].

MCrAlY coatings produced using this method usually have uniform thickness and superior density. Coatings deposited by EB-PVD are also very smooth, a necessity for proper air flow in turbine systems.

The technique of plasma spraying has been utilized for several decades. It can be used to deposit metals, ceramics or a mixture of the two. Microstructures of materials deposited by plasma spraying have very fine, equiaxed grains and are very uniform. To achieve good adhesion from plasma spraying, it necessary to roughen the surface through grit blasting, or other methods, before deposition. The process itself involves an approximately 40μm powder being introduced into the hottest section of a plasma gun, pictured in Figure 6. The particles melt in the flame and are propelled to the substrate where they splat on the surface and undergo rapid cooling and solidification. This process continues building up the coating until the desired

thickness is obtained. Coatings of virtually any thickness can be produced in this manner. For critical applications, such as turbine systems, this process may be carried out using an argon or nitrogen shrouded flame to prevent oxygen from reaching the flame or the substrate. This can help to improve the density as well as the coating adhesion. The density of the coatings can also be improved by increasing the particle velocity. This can be achieved using vacuum plasma spraying which is performed in a vacuum chamber at approximately 50-200 mbar [10].

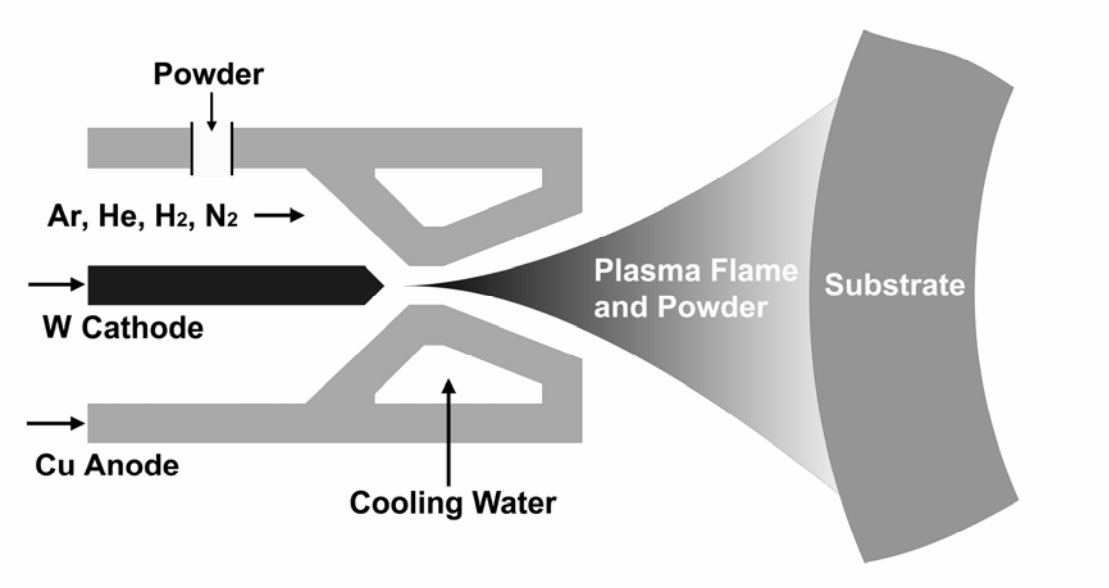

Figure 6. Schematic of Plasma Spray Apparatus [4].

2.2.4 Reactive Element Effect

As was mentioned previously, it has been found that the addition of small amounts of reactive elements, such as yttrium, can significantly enhance the oxidation resistance of high temperature alloys [13]. The reason for this is not completely understood. Both alumina and chromia-forming alloys can benefit from the addition of these elements, which also include cerium and hafnium. The main improvements in the oxidation behavior arise from increased adherence of the thermally-grown oxide and a decrease in the growth rate of the oxides [14]. Improving these characteristics leads to better thermal cycling resistance of the oxides. The effect is usually more pronounced in chromia forming alloys, where the oxide grain size is often decreased in addition to the improved adherence and a decrease in oxide growth rate is observed [15]. Figure 7 illustrates the reactive element effect for Ni-Cr-Al alloys under cyclic oxidation conditions. It can be seen that the lifetime of the alloys is greatly increased by the addition of Y and Hf.

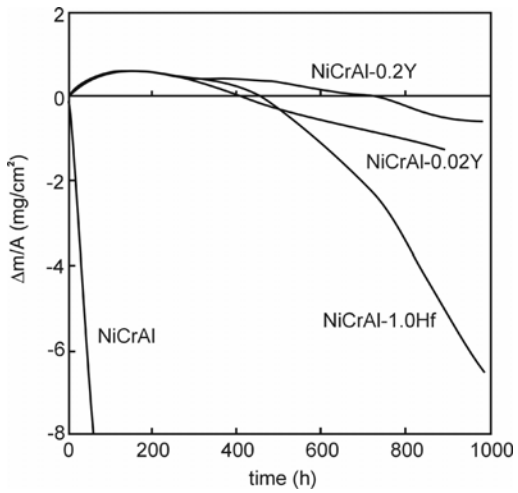

Figure 7. Cyclic oxidation kinetics for model Ni-Cr-Al alloys exposed at 1100°C [16].

Many theories have been developed in an attempt to understand these improvements. Mechanisms that have been suggested to explain the reduction in scale growth rate include doping effects, formation of a blocking layer in the scale and blocking short-circuit diffusion [14]. Effects on alumina have mostly been ignored as there is little evidence that reduced oxide growth rate is observed in alumina formers. In 1965 it was suggested that adding 1% yttrium to an iron-chromium alloy would result in a slower oxide growth rate due to a modification in the chromia structure causing the rate of cation diffusion through the scale to be reduced [17]. Since both Y and Cr are trivalent, it is unlikely that a doping effect would occur. It is possible that choosing a reactive element with a different valence, such as thorium or cerium could alter the rate of transport.

A theory involving a blocking layer of a compound of the reactive element yttrium in Fe-Cr alloys was suggested by Wood and Boustead in 1968. This theory assumes the formation of a continuous layer of a compound such as $YCrO_3$ or Y_2O_3 at the alloy-scale interface. They were unable to discover a continuous layer, but detected a Y-rich compound along half of the alloy-scale interface [18]. It is thought that this layer could act as a barrier to diffusion, thus slowing the rate of oxidation.

The short circuit diffusion model suggests that there is a segregation of yttrium to the grain boundaries during sintering of alumina that has been doped with yttrium. The presence of the yttrium will inhibit the short circuit diffusion that usually occurs along the grain boundaries, limiting the transport and decreasing the oxidation rate [19].

Mechanisms that assist in improving scale adherence are modifications to the growth process, enhanced scale plasticity, a vacancy sink model, improved chemical bonding, a graded seal mechanism, oxide pegging and a low-sulfur theory [4].

One theory involving modifying the growth process suggests that by reducing the growth rate, reactive elements can cause a reduction in the compressive stresses in the oxide, thus reducing spallation [20]. A 1996 study from the University of California tested this hypothesis by mapping oxide stress development in three alumina forming alloys with and without additions of yttrium. It was found that Y did not decrease the residual compressive stress in the oxide scales. Results indicated that, for short oxidation times, greater compressive stresses were experienced by the yttrium-doped samples [21].

The hypothesis of enhanced scale plasticity suggests that the reactive elements cause alumina to become more deformable, improving adhesion by reducing various stresses in the oxide scale. This idea arises from the fact that deformation in the scale primarily occurs by grain boundary sliding. If yttrium additions were to create a finer-grained microstructure, the grain boundary sliding could be more easily accommodated [22]. It is alternatively suggested that yttrium actually worsens the scale plasticity because yttrium compounds form in the grain boundaries inhibiting grain boundary sliding [23].

The vacancy sink model, states that the reactive elements act as vacancy sinks, preventing voids from forming at the alloy oxide interface in alumina forming alloys [22]. By reducing the concentration of voids at the interface, a greater proportion of the scale can remain in contact with the alloy and reduce spallation. This suppression of void formation was verified by Allam *et al.* [12] who noticed that voids were completely eliminated in a cobalt-chromium-aluminum alloy when 0.5% Y or Hf was added. The voids did return after long exposure times, but these too were eliminated when the reactive element concentration was increased suggesting that the vacancy sinks can become saturated [24].

The graded seal mechanism is based on differences in the coefficient of thermal expansion (C.T.E.) between the substrate and the oxide. This theory implies that if a reactive element oxide with an intermediate C.T.E. forms between the alloy and the scale, spallation due to C.T.E. mismatch could be minimized [25]. However, as was mentioned previously in the case of a blocking layer to decrease scale growth rate, a continuous layer of compound oxide has not been observed.

A theory suggested by many sources is the idea of oxide pegging, in which pegs form in the oxide at the scale-alloy interface to help anchor the oxide in place. It seems that, in alumina formers, the pegs consist mainly of Al_2O_3 growing into the substrate around the reactive element oxide [24]. Tien and Pettit studied the effect of oxide pegging on scale adherence in FeCrAlY and FeCrAlSc alloys. They found that oxide pegging did not greatly improve adherence, as in both alloys, no oxide pegs were maintained during the entire oxidation process but the scale remained adherent [22].

A slightly more recent theory that is generally accepted as having some role in improving oxidation behavior is the idea that reactive elements tie up sulfur in the alloy, preventing it from segregating to the metal surface. This segregation can lead to a weakening of the bond at the metal-oxide interface. Reactive elements are generally strong sulfide formers causing them to react with the sulfur present in alloys. Studies were performed by Funkenbusch *et al.* [26], who examined seven NiCrAl alloys with various additions of Y and Y_2S_3 separately and combined in various concentrations. Cyclic oxidation tests of the alloys were performed to test the proposed mechanism. The results showed that the baseline alloy with no additions lost weight due to spallation. The addition of elemental Y increased scale adherence and caused a mass increase. Addition of Y_2S_3 caused a large mass decrease. Adding elemental Y and Y_2S_3

caused mass increase and improved adherence. Auger spectroscopy was used to determine that very high surface concentrations of S are present in alloys with a small bulk composition of S. Both of these results seem to support the proposed mechanism [26], [27]. Also, studies performed in which sulfur content has been reduced through H_2 annealing have produced good adherence with no reactive element present.

2.2.5 Surface Preparation Effects

The surface condition of the coatings when they are exposed to oxidizing environments has been shown to play an important role in their lifetimes. Different deposition methods can produce wide variations in the surface roughness of MCrAlY coatings. Surface treatments that may be performed on coating surfaces include hand-polishing, rough grinding, and grit blasting.

Recent studies have shown that in NiCoCrAlY coatings exposed in their rough, as-sprayed state at 1100°C, the alumina scales had a completely different morphology than those grown on a coating surface that had been ground flat [3]. The scale formed on the flat surface had a uniform thickness and a homogenous distribution of Y-Al mixed oxide precipitates beneath the surface of the coating. In the convex areas of the rough coating (R_a~10μm), the scale was thinner with few Y-Al precipitates. There was also formation of the less-protective spinel on the surface of the convex areas. In the concave regions, there was no spinel formation and the oxide layer was thicker with many more Y-Al precipitates. These differences can be explained through the idea of the diffusion distance of the Y. On both the rough and the smooth coating, Y is preferentially oxidized beneath the surface. Once the Y below the surface is depleted, Y must diffuse from the bulk of the coating to continue the formation of the yttrium-aluminates. In the

smooth coating, the diffusion distance is the same for the whole length of the coating, but in the rough surface, the diffusion distance is much shorter for Y traveling to the concave regions and much greater for Y traveling to the convex regions. This explains why significantly more Y-Al precipitates were observed in the concave regions. The lack of incorporation of yttrium was believed to lead to enhanced spallation of the alumina scale in the convex regions, leading to earlier coating failure.

Similar surface treatments have also been studied in PtAl systems, but the results of different studies have been somewhat contradictory. The most common surface treatment for PtAl coatings is grit-blasting, especially in PtAl's used as bond coats for thermal barrier coatings (TBC's).

One study found that grit-blasting the PtAl coatings for use in TBC systems led to the introduction of various impurities into the surface from the grit-blasting media [28]. The authors concluded that when the grit-blasted coatings are oxidized, the impurities lead to rapid acceleration of the alumina growth rate, leading to earlier spalling the scale. On samples tested without grit-blasting on the as-aluminized surface, it was found that the alumina scale had a much slower growth rate and exceptional resistance to spalling in cyclic tests. This would seem to indicate that grit-blasting is causing premature failure in PtAl and TBC systems.

Another study on the issue suggests that voids located beneath the alumina scale on PtAl's are responsible for the early failure of many TBC's [29]. Here it was found that voids were not present in coatings that had undergone grit-blasting and that this effect was due to the removal of surface impurities, such as sulfur, and the acceleration of α-Al_2O_3 formation. This study appears to indicate that any surface treatment that can remove excess sulfur and accelerate

α-Al_2O_3 formation, without adding to surface roughness, would likely increase the lives of PtAl coatings.

2.3 COATING DEGRADATION AND FAILURE

Testing the performance of coatings in the laboratory under conditions similar to those they would experience in use is critical to the safe use of the materials. Numerous tests are available to closely simulate the working environment of high temperature coatings and to characterize their failure mechanisms.

Many materials systems, and nearly all turbine systems, are subjected to cyclic exposure conditions throughout their lifetimes. In isothermal conditions, the amount of material being consumed is controlled by the rate at which oxidation proceeds. Isothermally grown oxides usually follow the parabolic rate law in which the oxidation rate is inversely proportional to the scale thickness. This means that the oxidation rate is controlled by the rate of diffusion through the oxide scale. In cyclic exposures, a cycle consists of a heat-up time, a hold at temperature, and a cooling-time. Failure under cyclic conditions usually occurs upon cooling, when spalling of the protective oxide layer can occur. Upon reheating, rapid oxidation will occur in the spalled regions, leading to substantial material degradation.

In addition to spalling, cracking of the coatings can occur under certain circumstances. For non-load bearing materials, cracking frequently occurs as a result of differences in thermal expansion coefficients between the coating and the substrate. Like spalling, this allows more rapid oxidation to occur once the sample is reheated and, in some cases, cracks may extend through the entire coating, providing a direct path for oxidation of the substrate.

One method of failure in PtAl coatings exposed to cyclic conditions is rumpling. Rumpling refers to a severe wrinkling of the coating during exposure. This occurs due to the differences in the coefficients of thermal expansion between the oxide and the coating and the coating and the substrate. The presence of rumpling can be minimized by smoothing the surface of the coatings prior to exposure [4].

Since coatings are so thin relative to the bulk substrate, there is a limited amount of material present to form protective oxides. In the case of MCrAlY and PtAl coatings, failure occurs when the coating is depleted of aluminum and the protective α-Al_2O_3 scale can no longer form. In MCrAlY coatings, the scale is formed by the consumption of the Al-rich β phase. At long times, the β at the scale-coating interface is consumed with the formation of the scale, and the β at the coating-substrate interface is lost to interdiffusion. This process continues until the β phase in the coating is completely consumed.

3.0 RESEARCH OBJECTIVES

This research was intended to extend the lives of coatings on superalloys that are exposed to cyclic oxidation conditions in gas turbine systems. This was accomplished by controlling the microstructure and adherence of an α-Al_2O_3 scale using several approaches. MCrAlY and platinum aluminide coatings were characterized after long exposure times at elevated temperatures to examine and understand the degradation process. The effects of surface roughness were studied by altering the surfaces of the coatings prior to exposure. Surface treatments included:

- Hand-polishing
- Media Finish
- Grit Blasting
- Etching

Finally, the effects of varying the concentration of the reactive element yttrium in the MCrAlY coatings were examined.

Based upon the results obtained in the long-term exposures, further studies were done, focusing on the coating surface conditions that produced the optimum performance.

4.0 EXPERIMENTAL PROCEDURE

The substrate used in this work was the Ni-base superalloy René N5, the composition of which is shown in Table 1. René N5 is a cast single crystal consisting of a gamma matrix with gamma prime precipitates.

Table 1. Alloy and Coating Composition (Weight %)

	Ni	Cr	Al	Co	Ta	W	Mo	Ti	Hf	Y	Re
René N5	Bal.	7	6.2	7.5	6.5	6	0.6	1	0.1		3
NiCoCrAlY	Bal.	16.5	12.6	21.8						0.1	
NiCoCrAlY	Bal.	16.5	12.6	21.8						0.5	

Three coatings were studied. Two were NiCoCrAlY overlay coatings, deposited by argon-shrouded plasma spraying, that were approximately 160 μm thick. As shown in Table 1, the compositions were nearly identical except that one coating contained 0.1 weight % yttrium and the other contained 0.5 weight % yttrium. The third coating was a platinum-modified aluminide coating produced by a high temperature low activity CVD process. In this process, the René N5 substrates underwent Pt electroplating to deposit 5-7 μm of Pt on the surface, followed by a heat treatment to allow interdiffusion of the Pt and the substrate. Aluminum was then deposited through a CVD process to produce a final coating thickness of approximately 40-50

μm. The samples were either circular disks with a 2.5 cm diameter or coupons that measured 1.5 cm x 1 cm. The thickness of the samples was about 3mm.

The three coating types were exposed after a variety of surface treatments. After coating deposition, all of the coatings were vacuum heat-treated, peened with stainless steel shot, and vibratory finished with alumina media. Some specimens were exposed in the as-received condition in which case the surface was not altered prior to exposure and the R_a varied between two and five microns. Other specimens were diamond polished on a Struers automatic polisher to an R_a of approximately 0.3 microns. Several specimens were light grit blasted in an Empire Basket Blaster for 30 minutes with 700 μm alumina at a pressure of 0.17 MPa. This resulted in an R_a of approximately 2μm. Some of the light grit blasted samples were then subjected to an NaOH etch to remove the imbedded blasting grit. This process also resulted in an R_a of 2μm. Figures 8-11 show surface SEM images of the various sample conditions. Following the surface treatments, all samples were ultrasonically cleaned in soapy water and then ultrasonically cleaned in acetone.

Most of the samples were exposed to cyclic oxidation conditions in a CM bottom-loading furnace in laboratory air. All of the tests were performed at 1100°C. Each cycle consisted of a ten minute heat-up period to 1100°C, a 45 minute hold at temperature, followed by a ten minute cooling period to approximately 100°C with forced laboratory air blowing on the samples. This furnace set-up is shown in Figure 12.

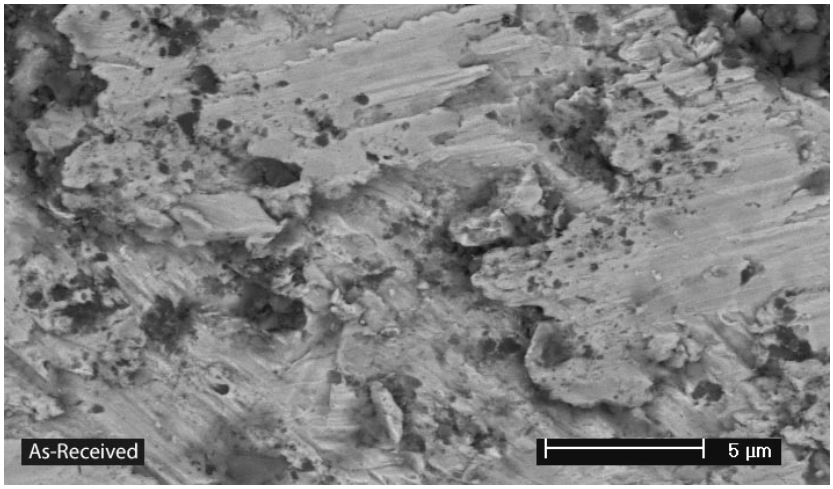

Figure 8. As-Received NiCoCrAlY Coating

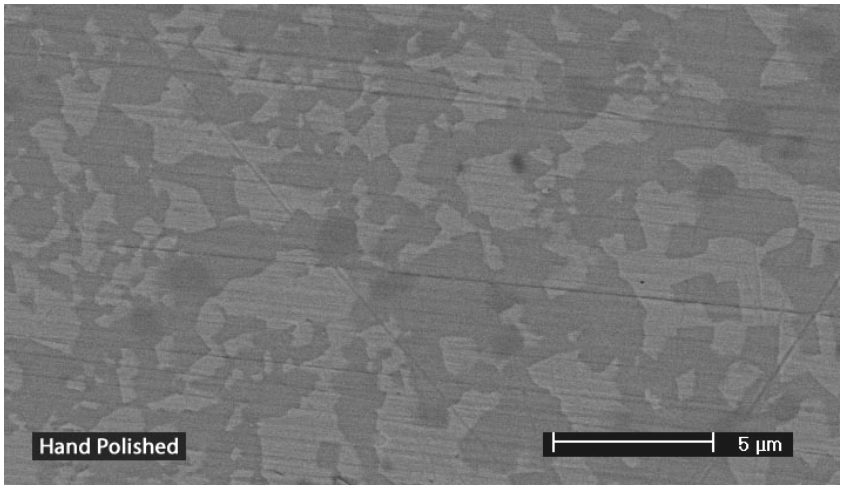

Figure 9. Hand Polished NiCoCrAlY Coating

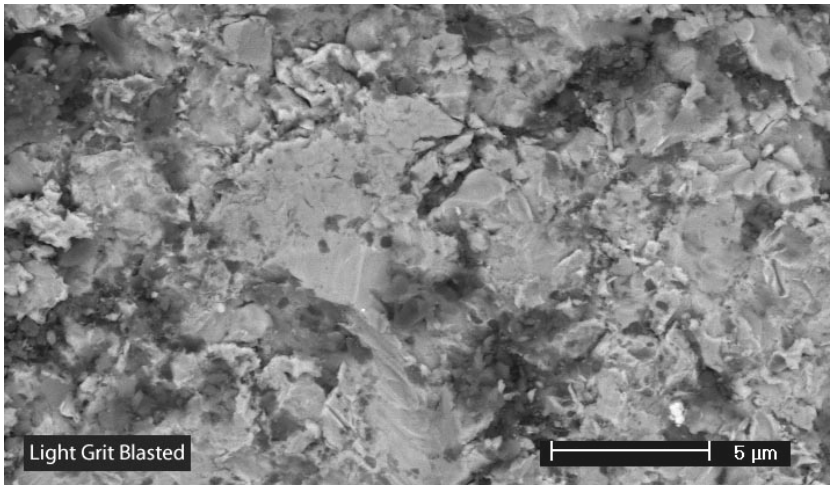

Figure 10. Light Grit Blasted NiCoCrAlY Coating

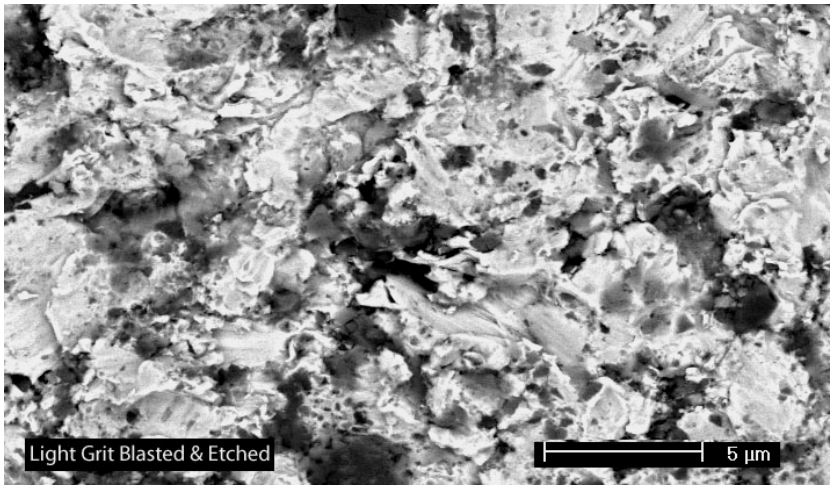

Figure 11. Light Grit Blasted & NaOH Etched NiCoCrAlY Coating

Figure 12. Bottom-Loading Furnace for Cyclic Oxidation Tests

Following the high temperature exposure of the samples, they were examined using optical and scanning electron microscopy (SEM) to analyze the performance of the coatings. The SEM used in this research was a Philips XL30 FEG (field emission gun). Both secondary electron (SE) and back scattered electron (BSE) detectors were used. Energy dispersive spectroscopy (EDS) was also performed to obtain chemical analysis of the coatings.

Several samples were chemically etched to further reveal microstructural characteristics. The etchant used was AG-21 which is composed of 50 ml. of lactic acid, 50 ml. of nitric acid, and 2ml. of hydrofluoric acid. Samples were swabbed with the mixture for 15 seconds and then rinsed with de-ionized water.

5.0 RESULTS AND DISCUSSION

5.1 CYCLIC OXIDATION RESULTS

Most of the NiCoCrAlY and PtAl coated samples were thermally cycled until severe degradation of the surfaces was observed. Some of the samples were removed at shorter intervals to obtain a complete picture of the events taking place in the system.

5.1.1 Cyclic Oxidation of NiCoCrAlY Coatings

The NiCoCrAlY samples containing 0.1 and 0.5 weight % Y were removed from thermal cycling every few hundred cycles. The surfaces were examined visually to note any signs of degradation and the samples were weighed. The weight changes for these samples are not very meaningful because the NiCoCrAlY coating is only present on one side of the sample. Samples were also removed occasionally, whether or not they showed signs of degradation, and examined on the SEM. Cross-sections of the as-received coatings prior to any exposure can be seen in Figures 13 and 14.

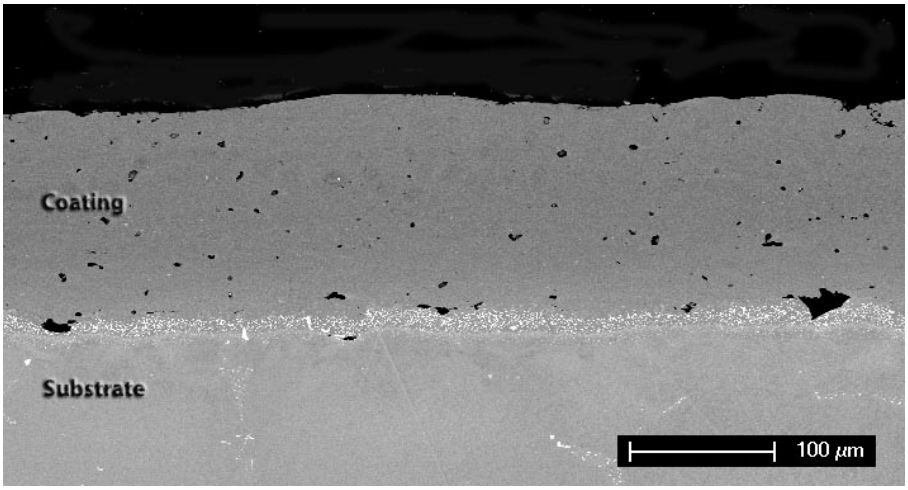

Figure 13. As-Received NiCoCrAlY Coating Containing 0.1 wt. % Y

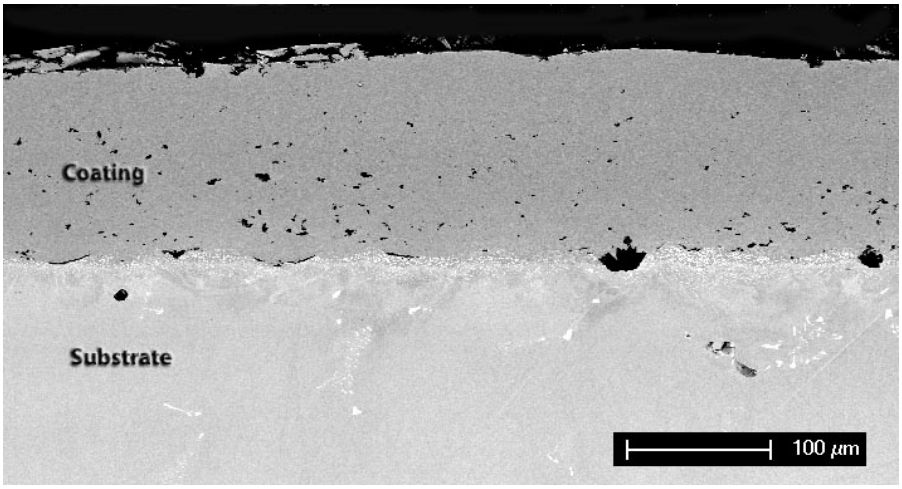

Figure 14. As-Received NiCoCrAlY Coating Containing 0.5 wt. % Y

Both the coating containing 0.1 wt. % Y and that containing 0.5 wt. % Y look similar prior to exposure. There is evidence of a small amount of porosity in both coatings. The large black particles at the substrate-coating interface are alumina particles left from when the substrate underwent grit blasting prior to the deposition of the coating. Higher magnification of one of the coatings, shown in Figure 15, reveals more of the underlying microstructure.

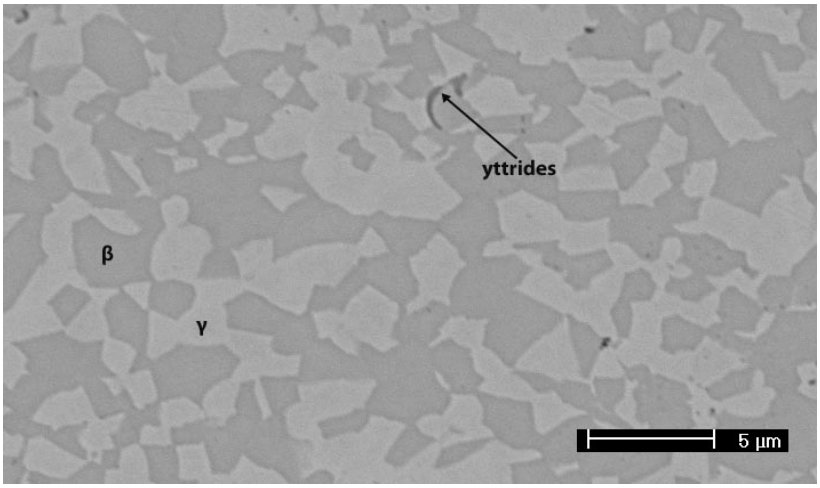

Figure 15. As-Received NiCoCrAlY Coating Containing 0.1 wt.% Y at High Magnification

The two phases in the coating are clearly visible in this image. The darker β-phase is rich in aluminum and provides an aluminum reservoir to encourage formation of α-Al_2O_3 on the coating surface. During long exposure times, the β-phase is slowly consumed until, eventually, none remains. Yttrides are frequently present on the β/γ phase boundaries, as seen in Figure 15.

In the first round of testing, the samples were weighed and examined every 200 cycles. After 2000 cycles at 1100°C, the first samples were removed and sectioned. A 0.1 wt.% Y and a

0.5 wt.% Y sample were removed. Both samples had been light grit blasted prior to exposure. The cross-sections of the samples are shown below.

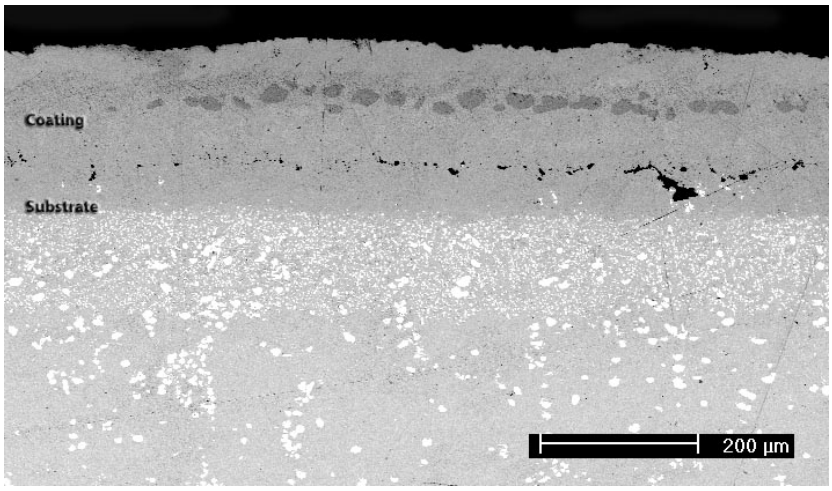

Figure 16. 0.1 wt% Y, LGB Sample after 2000 Cycles

After 2000 cycles, the light grit blasted sample containing 0.1 wt.% Y has a slightly irregular surface, but exhibits no major damage to the coating. A good amount of the dark β-phase is visible running through the middle of the coating. The coating containing 0.5 wt.% Y is shown in Figure 17. This sample had numerous protrusions extending into the coating and the β-phase was not apparent. The protrusion in Figure 17 is shown at higher magnification in Figure 18. In Figure 18, the alumina filling the protrusion is visible. It is seen to have a layered appearance, which may be due to cracking during the cyclic exposure. A few of the protrusions in this sample completely penetrated the coating and began to extend into the substrate. One of these protrusions is shown in the Figures 19 and 20.

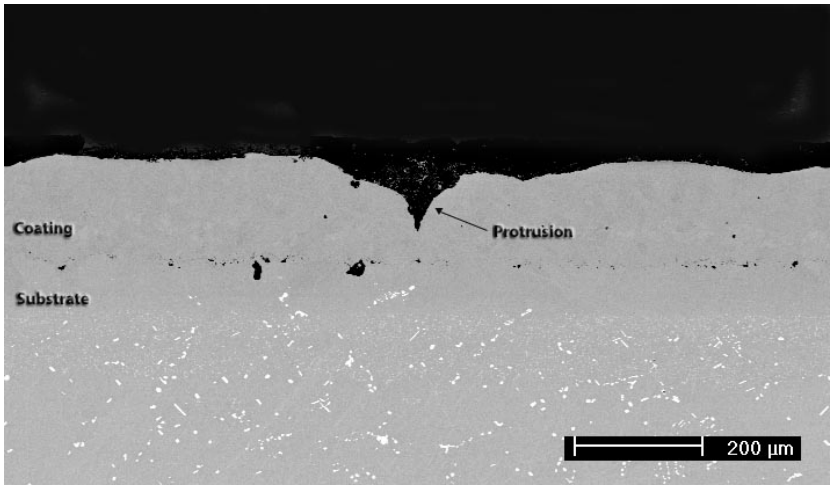

Figure 17. 0.5 wt% Y, LGB Sample after 2000 Cycles

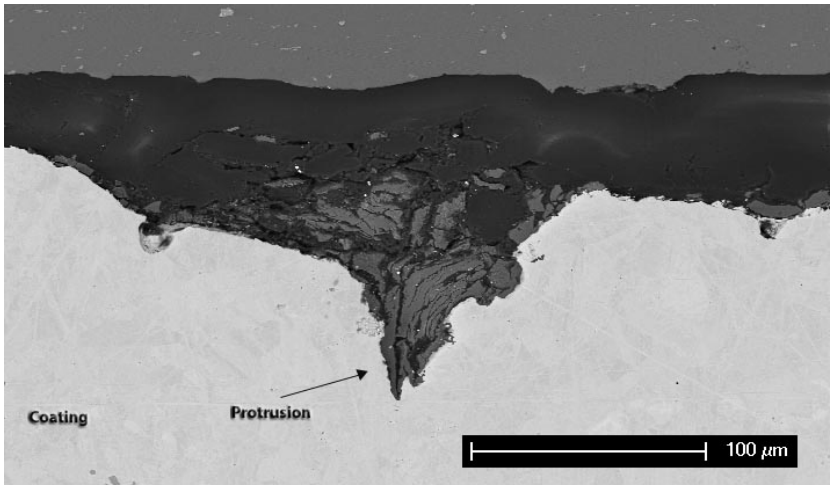

Figure 18. Protrusion in 0.5 wt.%, LGB NiCoCrAlY Coating after 2000 Cycles

Figure 19 shows the protrusion spreading out when it reaches the original interface between the substrate and the coating, marked by the presence of alumina grit blasting particles. At higher magnification in Figure 20, particles containing yttrium are observed surrounding the tip of the protrusion. Yttrium in the coating has been found to segregate to this interface and the protrusions appear to grow more rapidly in the presence of large amounts of yttrium. The oxide in the protrusion contained a very small concentration of Y, but was primarily pure Al_2O_3. These yttrides have a clearly different appearance and morphology from those seen in Figure 15 in the un-exposed coating. This agglomeration of yttrium is not fully understood, but it is possible that in addition to the visible yttrides in the un-exposed coating, some yttrium is present in solution in the β-phase. As the β-phase is consumed, the solubility for Y is exceeded and yttrides (Ni-Y compounds) precipitate out and coarsen.

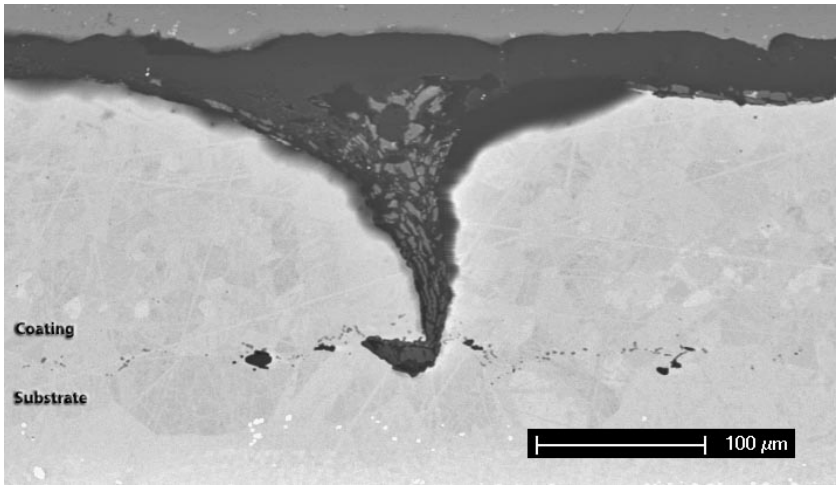

Figure 19. Protrusion Extending through Coating into Substrate

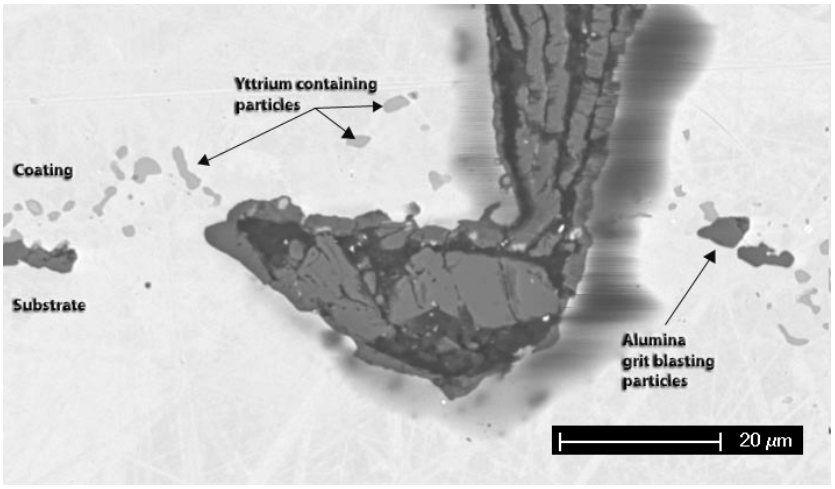

Figure 20. Protrusion Penetrating Original Interface

After only 200 cycles, the samples containing 0.5 wt.% Y were observed to be forming a network of blue colored oxide on their surfaces, while the 0.1 wt% samples remained gray. This blue oxide has been found to correspond to the areas where protrusions were seen in cross-section. Figure 21 shows surface scans of two samples that were removed after 2800 cycles at 1100°C. Both samples had been light grit blasted and then etched with NaOH to remove the grit blast particles prior to exposure. One sample contained 0.1 wt.%Y and the other 0.5 wt.% Y. The network of blue oxide on the sample containing 0.5 wt.% Y is clearly visible in Figure 21. Cross-sectional images of the two samples are shown in Figure 22. Severe damage, namely oxidation and cracking, has occurred in the sample containing 0.5 wt.%Y, while the 0.1 wt.% sample still appears fairly planar. There is still some β-phase remaining in the sample containing 0.1 wt.%Y. This seems to imply that the presence of blue oxide on the surface indicates that the coating is no longer fully protective and that severe degradation may be taking place.

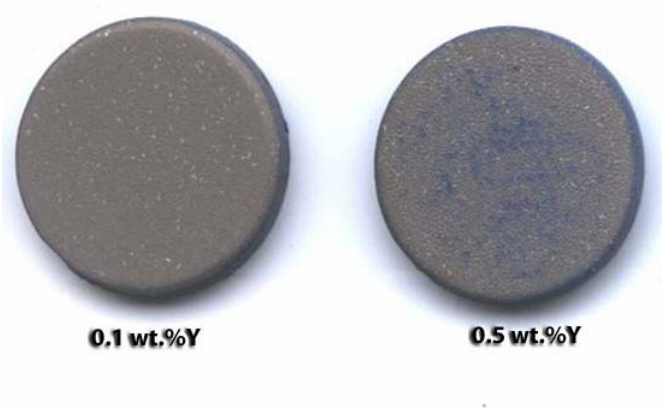

Figure 21. Surface Images of Sample Surfaces after 2800 Cycles

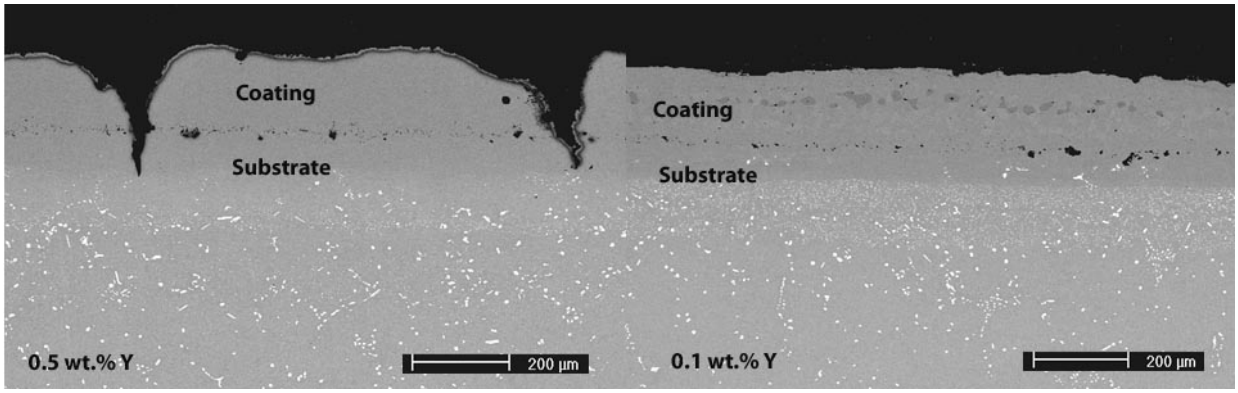

Figure 22. Comparison of 0.5 and 0.1 wt.% Y Coatings after 2800 Cycles

Previous surface scans had shown a difference in the oxidation behavior of the hand polished samples containing 0.5 wt.% Y when compared to other surface treatments. One of these images is shown below, in Figure 23. Both samples contained 0.5 wt.%Y, but one had been light grit blasted and etched, and the other had been hand polished. While the light grit blasted and etched sample displays the characteristic blue oxide seen on the other 0.5 wt.% Y samples, the hand polished surface remains planar and gray. Cross-sections of the two samples were compared to look for protrusion formation in the hand polished sample.

As might be expected from the surface images, Figure 24 reveals that the coating that was light grit blasted and etched has sustained substantial damage, with protrusions penetrating the entire coating. While one small protrusion is visible on the hand polished sample, it is far from penetrating the coating and the rest of the surface appears smooth. This shows that while the higher yttrium content appears to be detrimental to the coating performance, hand polishing reduces or eliminates these effects.

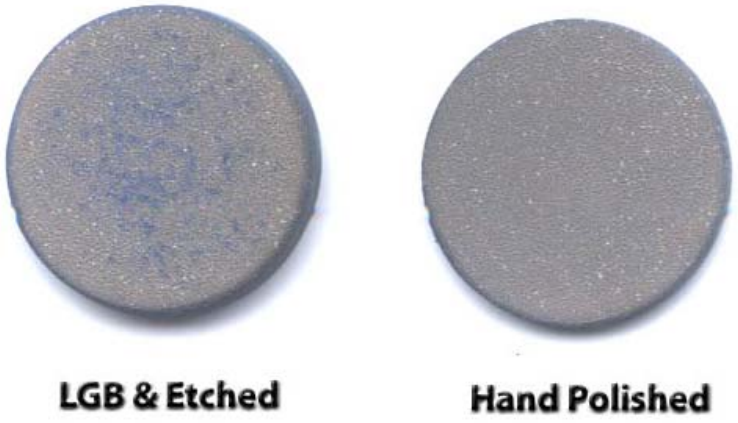

Figure 23. Comparison of Surface Treatments in 0.5 wt.%Y Coatings after 2800 Cycles

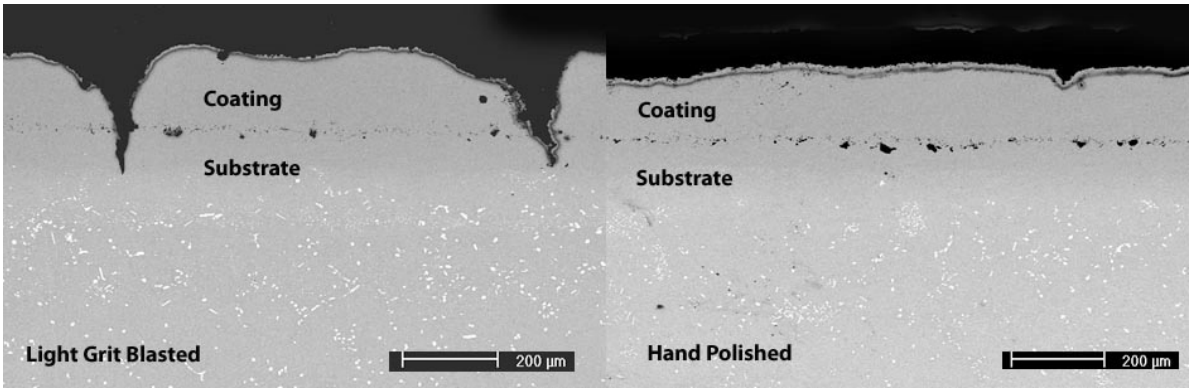

Figure 24. 0.5 wt.%Y Coatings with Different Treatments after 2800 Cycles

Samples removed after 3700 cycles at 1100°C continued to follow the trend of the previous coatings. Figure 25 shows surface scans of two as-received coatings with different yttrium contents. The blue oxide in Figure 25 has formed a continuous network over almost the entire coating surface of the 0.5 wt% sample. Cross sectional images of this sample are shown below.

Figure 26 shows the cross section at low magnification. It can be seen that numerous protrusions are visible and that they have completely penetrated the coating. Higher magnification of one the protrusions is shown in Figures 27 through 29.

Figure 25. Surface Images of Sample Surfaces after 3700 Cycles

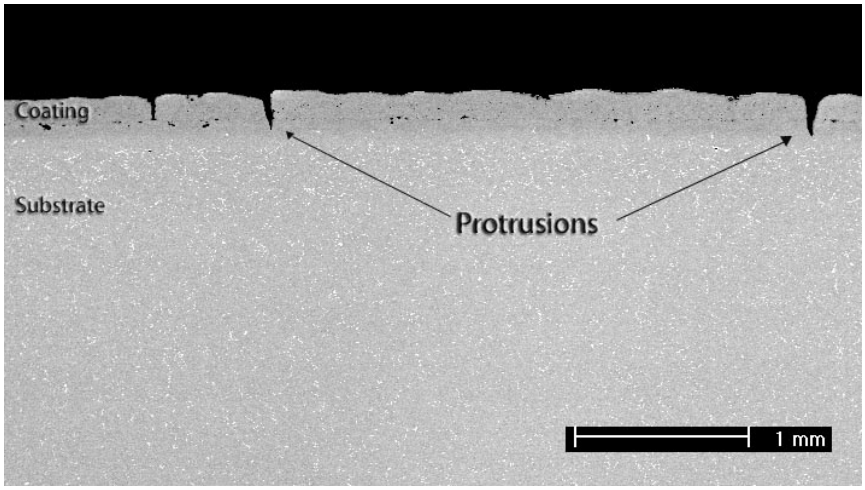

Figure 26. Cross section of LGB 0.5 wt.% Y Sample after 3700 Cycles

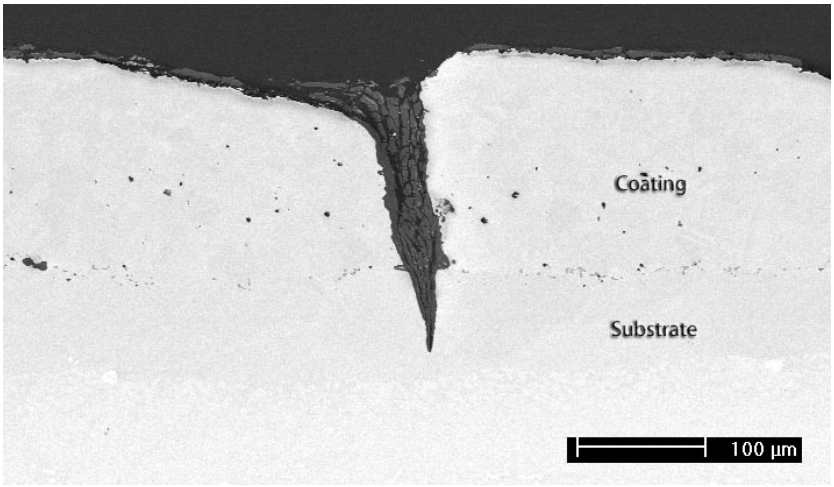

Figure 27. Protrusion in 0.5 wt% Y Coating after 3700 Cycles

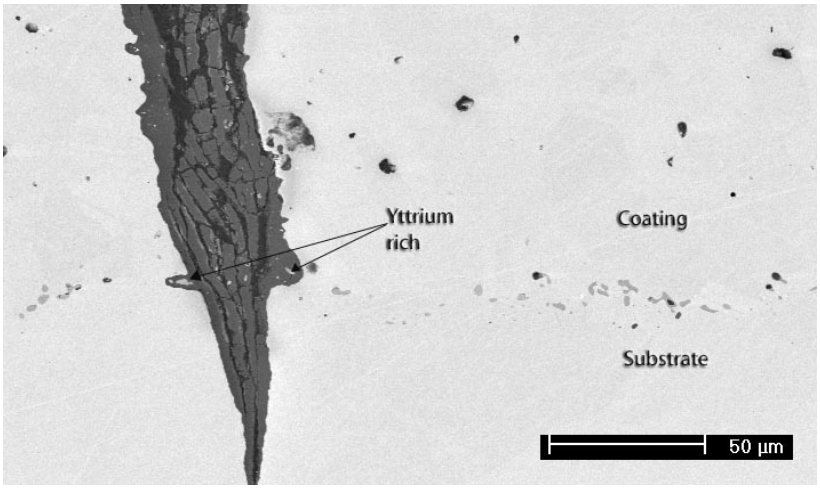

Figure 28. Yttrium rich Particles in Protrusion

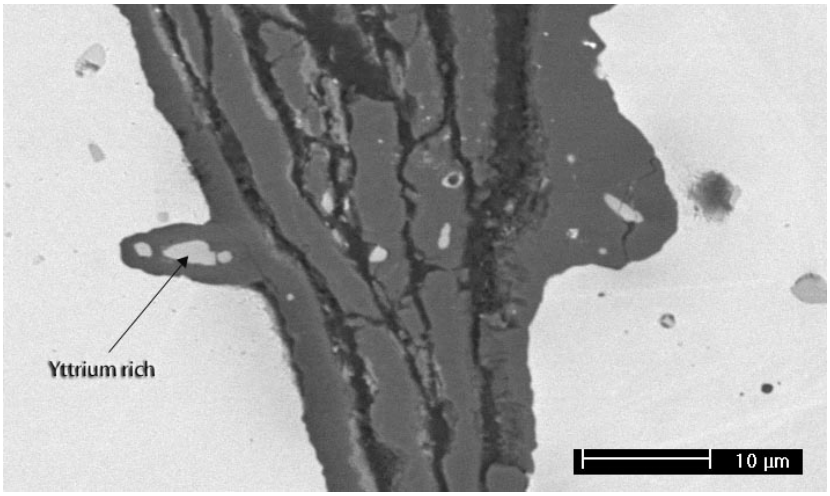

Figure 29. High-Magnification Image of Protrusion

The protrusion is filled with Al_2O_3 which exhibits the same cracking that was observed in previous samples. Yttrium-rich particles are also seen surrounding the coating and incorporated into the oxide. Figure 29 shows very well at high magnification that the protrusion develops "side-arms" and begins to spread out once it reaches the original interface where a large concentration of yttrium rich particles is present.

Another protrusion from the same sample is shown in Figures 30 through 32. This protrusion has a slightly different morphology as it does not have a pronounced tip. Once again, in Figure 31, it can be seen that yttrium has been incorporated into the alumina and appears to be dispersed throughout the scale. Figure 32 shows the surface of the protrusion and is labeled to show areas where $NiAl_2O_4$ and $CoAl_2O_4$ (spinels) are present. These spinel compounds are responsible for the blue color observed on the surface of the samples containing 0.5 wt.% Y. It is likely that the spinel forms as a result of increased Ni and Co activity in regions of the coating where the aluminum has been consumed in large quantities.

It is apparent that protrusions are present only in the samples containing 0.5 wt.% Y and that in these samples there is usually a large concentration of yttrium rich particles in the areas immediately surrounding the protrusions. Since the 0.1 wt.%Y samples are showing no evidence of protrusions, it is assumed that the increased yttrium content in the 0.5 wt.% samples is having a detrimental effect.

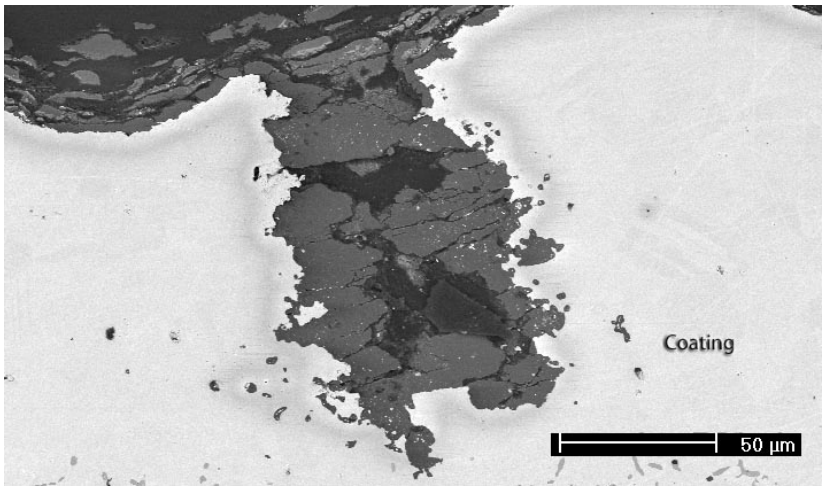

Figure 30. 0.5 wt.% Y, As-Received Coating after 3700 Cycles

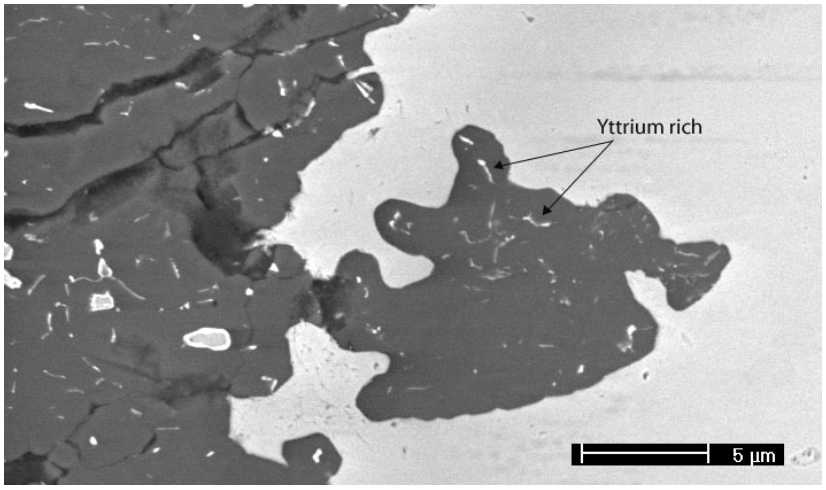

Figure 31. Yttrium rich Particles Incorporated into Oxide in Protrusion

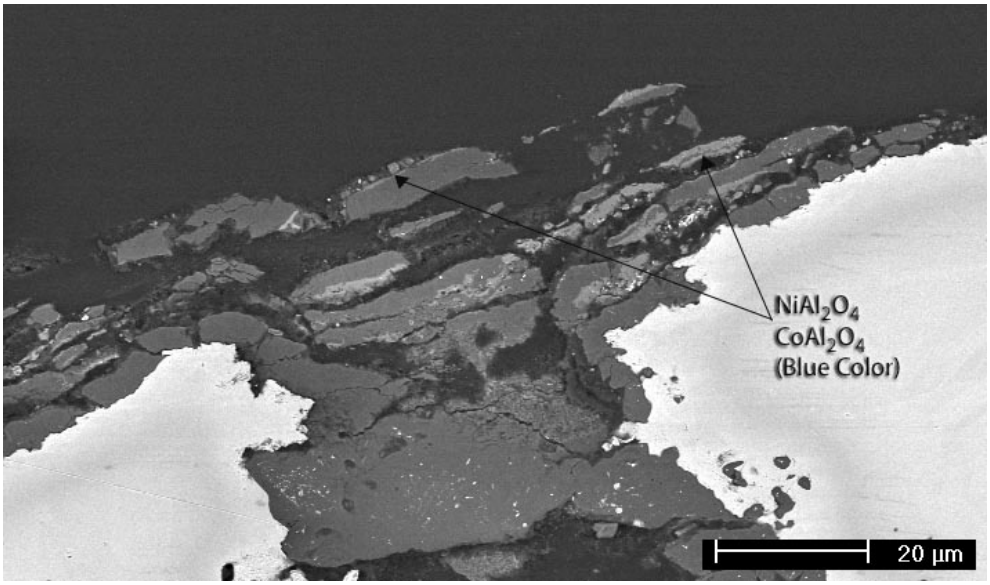

Figure 32. Spinel at Surface of Protrusion

A hand polished sample containing 0.5 wt. %Y was also removed after 3700 cycles. Cross sections of the hand polished sample were examined to ensure that no protrusions were forming. In Figure 33, a few very small protrusions can be seen, but the surface is otherwise smooth. This is in contrast to Figure 26 which shows deep protrusions in the light grit blasted sample after the same amount of time. The protrusions also have a completely different morphology than those seen in previous samples containing 0.5 wt.%Y. A higher magnification image of one of the protrusions can be seen in Figure 34. The protrusion is very rounded and is lined with a layer of alumina that is roughly five microns thick. Yttrium rich particles have also been incorporated into the oxide is several areas.

Also after 3700 cycles, a hand polished sample containing 0.1 wt.%Y was removed from test and cross-sectioned. These images are shown in Figures 35 and 36. Figures 35 and 36 both show no protrusions present in this sample. In Figure 36, the sample had been etched to emphasize the β-phase still present in the coating. Unlike the samples containing 0.5 wt.% Y, the 0.1 wt.% sample still has quite a bit of protective β-phase still present in the coating.

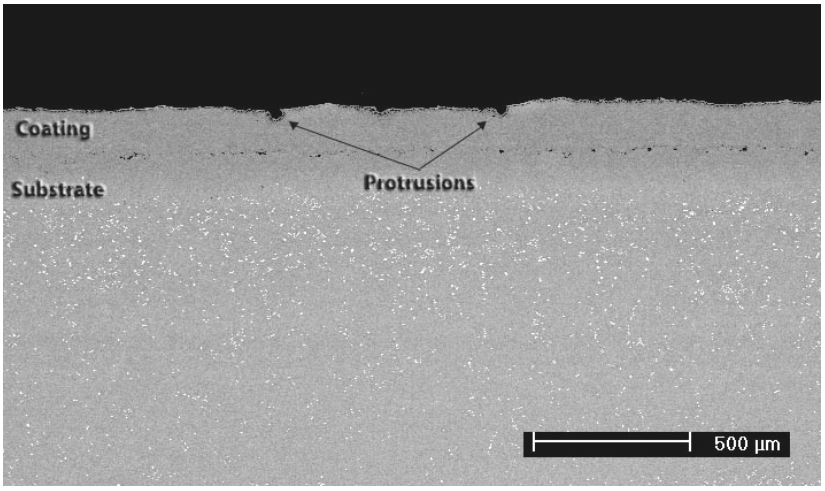

Figure 33. 0.5 wt.% Y, Hand Polished after 3700 Cycles at 1100°C

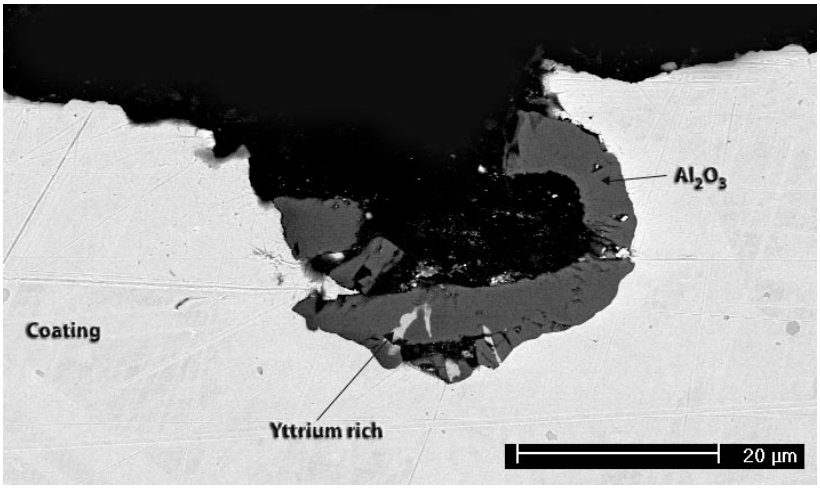

Figure 34. Small Protrusion in 0.5 wt.% Y, Hand Polished Coating after 3700 Cycles

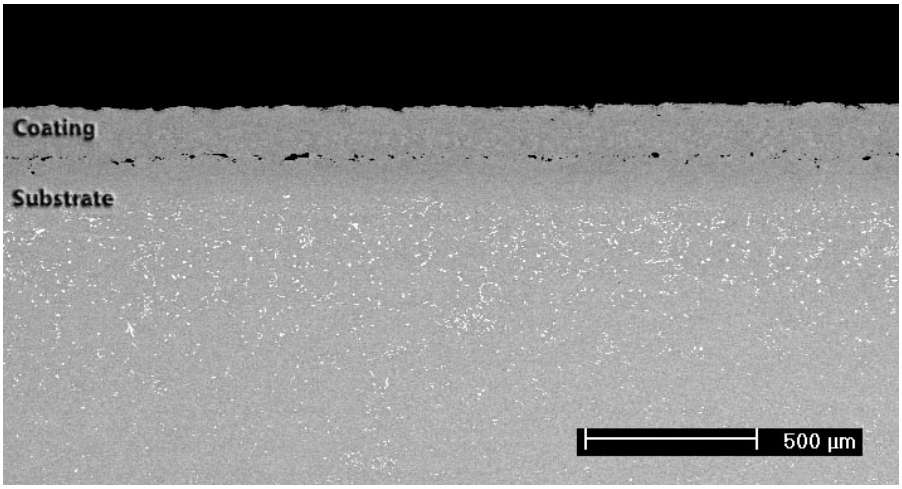

Figure 35. 0.1 wt.% Y, Hand Polished after 3700 Cycles at 1100°C

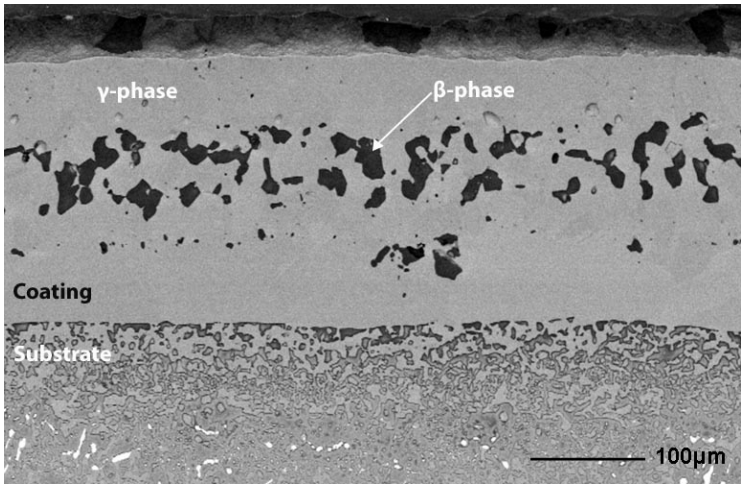

Figure 36. Hand Polished 0.1 wt.%Y Sample in Figure 35 Etched to Show β-Phase

After 3700 cycles at 1100°C, all of the samples containing 0.5 wt.% Y showed signs of excessive degradation and coating failure and were thus removed from test. Several samples containing 0.1 wt.% Y were left in test. After 5000 cycles, a hand-polished sample was removed and cross-sectioned. The surface of the sample was still completely gray and showed no signs of the blue oxide that had been observed on the 0.5 wt.% Y samples.

Figures 37 and 38 show that the hand polished coating exhibits no protrusions even after 5000 cycles at 1100°C. It appears that the coating is still approximately 100 microns thick. After very long times at high temperature, the β-phase appears to be converted to γ'. This is the lighter phase that can be seen clearly in Figure 38. During the initial stages of oxidation of this coating, the β-phase is converted to γ-phase as aluminum is removed from the coating. The observed, apparent conversion of the β-phase to γ'-phase may occur due to substantial changes in the composition of the coating due to interdiffusion with the substrate.

After 6500 cycles, another 0.1 wt.%Y sample was removed. As before the surface remained gray and planar. Figure 39 and 40 show the sample in cross-section. This sample also shows no protrusions and, as is seen in Figure 40, has a very adherent alumina layer approximately five microns thick.

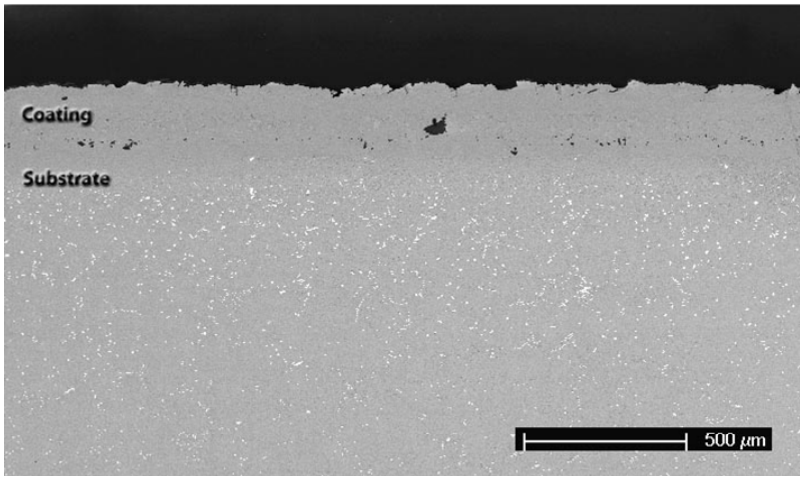

Figure 37. Hand Polished Coating with 0.1 wt.% Y after 5000 Cycles

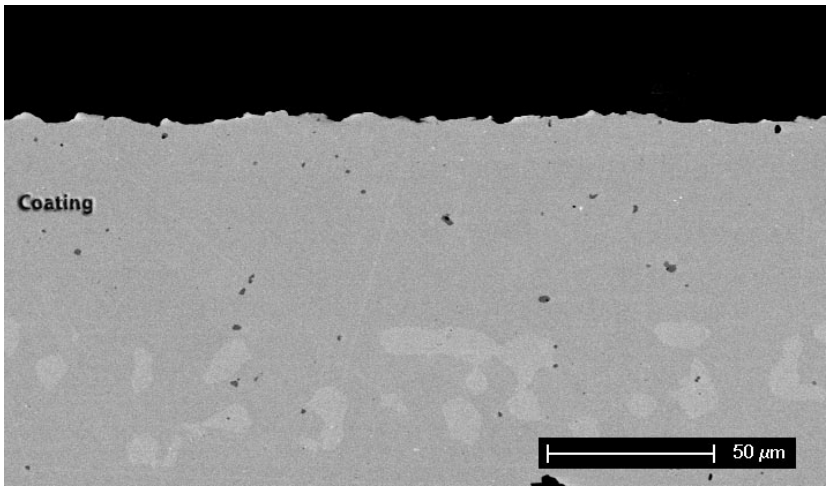

Figure 38. High Magnification of HP Coating with 0.1 wt.% Y after 5000 Cycles

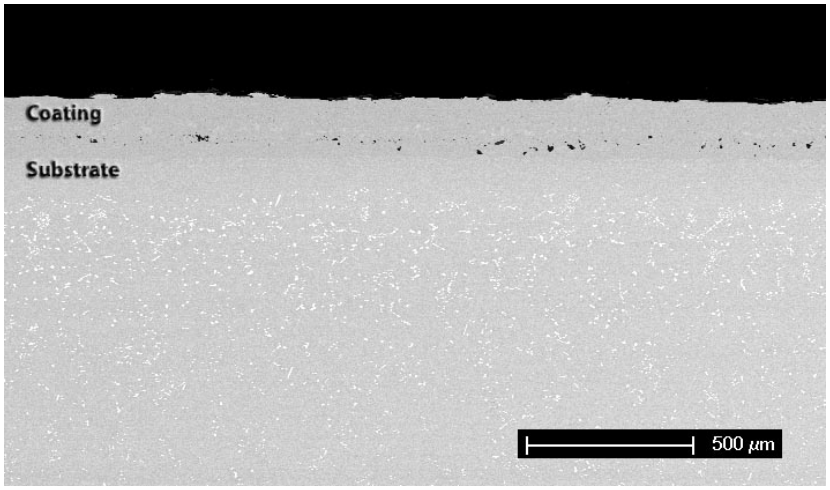

Figure 39. As-Received Coating with 0.1 wt.% Y after 6500 Cycles

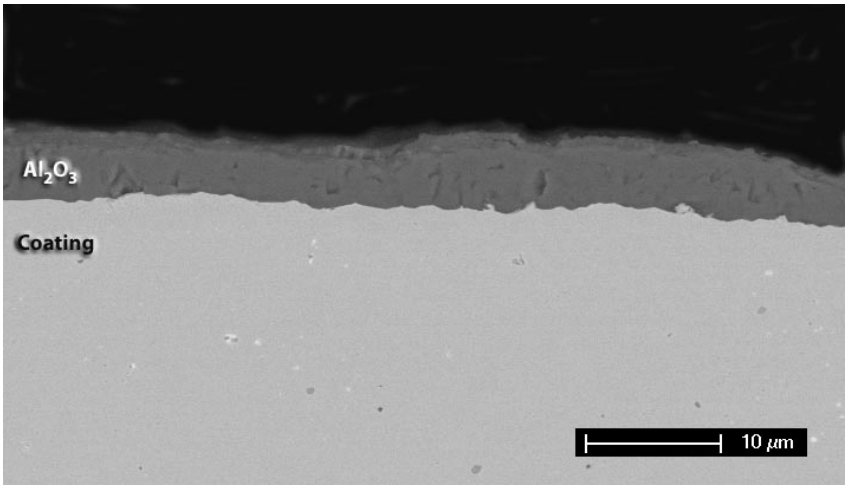

Figure 40. TGO on As-Received Sample after 6500 Cycles

Two other samples containing 0.1 wt.%Y will be left in test until they fail and at this point have undergone approximately 7500 cycles at 1100°C with no signs of failure or blue oxide formation on their surfaces.

From the above results, it is clear that deep oxide protrusions form in the samples with higher yttrium content that have rough surfaces, but do not form in the coatings with lower yttrium content for any surface condition. Also, hand polishing of the higher-Y content coating prevents the formation of these deep protrusions. Figure 41 shows a diagram of how these protrusions may form in the coatings with 0.5 wt.% Y that have rough surfaces. In the as-processed condition, the coating is made up of a matrix composed of γ and β-phase, with yttrides present around the regions of β-phase. Upon oxidation, yttrides near the surface preferentially oxidize and the yttrium rich protrusions form. As oxygen diffuses inward through the protrusion, yttrium from the bulk of the coating continues diffusing toward the surface and the protrusion grows.

Upon further cyclic oxidation, cracking is observed in the protrusion. Protrusions with a supply of yttrium and aluminum from the bulk, for example those near a grain boundary, will continue to grow until eventually the coating has been penetrated. This is shown in Figure 42.

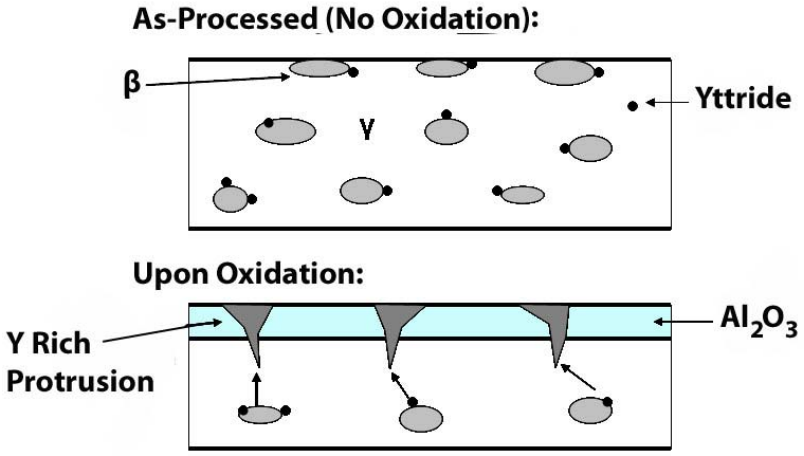

Figure 41. Protrusion Formation in NiCoCrAlY Coatings with Rough Surfaces

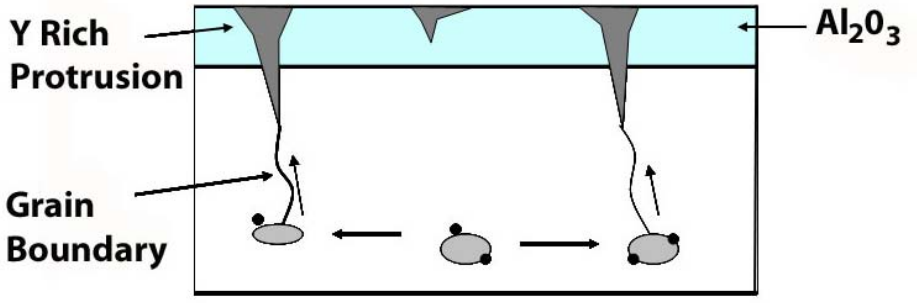

Figure 42. Advanced Protrusion Formation

This model implies that the amount of yttrium available to oxidize in the vicinity of the coating surface is very important. The fact that protrusions did not form in the samples with 0.1 wt.% Y implies that these samples did not contain enough yttrium to allow preferential oxidation of the yttrium and protrusion formation.

To explain the reasons that the 0.5 wt.% Y samples that were hand polished did not form protrusions, it is necessary to consider the concept of diffusion distance. Recently, studies performed by Gil et al [3] showed that Y rich protrusions form preferentially in the concave areas of rough NiCoCrAlY coatings when they are exposed to oxidizing conditions. This study concludes that there is a larger flux of yttrium to the concave regions because of their larger surface area, as well as the fact that the diffusion distance for the yttrium in the bulk is shorter traveling to a concave region as opposed to a convex region. These results are consistent with the present study. By fine polishing the surfaces of the 0.5 wt.% Y samples, the concave and convex regions were eliminated, promoting a more even distribution of yttrium beneath the surface of the sample.

As was previously mentioned, after long cyclic oxidation exposures, some of the protrusions had completely penetrated the coating. The method by which the protrusions propagate through the coatings is not completely understood, but an attempt will be made to explain this. The morphology of the protrusions, as well as the alumina observed in the protrusions suggests that cracking is taking place in the later stages of protrusion propagation. There is a significant difference in the coefficient of thermal expansion (CTE) between the substrate and coating, and the coating and the oxide. The CTE for the NiCoCrAlYs currently

being studied is approximately 17 x 10^{-6}/°C [30]. That for the René N5 substrate is roughly 14 x 10^{-6}/°C [30]and the average CTE for alumina at these temperatures is
9 x 10^{-6}/°C [31] . Examination of these values reveals that during cooling in cyclic oxidation, the presence of an alumina filled protrusion would result in tensile stresses in the surrounding coating. Although cracks have not been observed in the metallic coating during this study, if cracking were to occur during the cyclic tests, further propagation of the protrusion could occur by oxidation at the crack tip.

In an attempt to reproduce the original results and to obtain data about the coatings at shorter times, another batch of samples was put into test. These samples had a different geometry than the first batch in that they were rectangular coupons with dimensions of 1.5x1.0 cm rather that the circular disks.

After 100 cycles at 1100°C, the first of the new samples were removed from testing. One sample contained 0.1 wt.% Y and the other contained 0.5 wt.% Y. Both were in the as-received condition, meaning they had no surface modification. The surface SEM images of these samples are presented below. The bright white areas in both figures indicate regions where the alumina has spalled down to the bare metal of the coating. While only one small area of spalling was observed in the coating with 0.1 wt.% Y, significant networks of spallation were observed in the coating containing 0.5 wt.% Y. After examining the surfaces of the coatings, the 0.5 wt.% Y coating was cross-sectioned and observed.

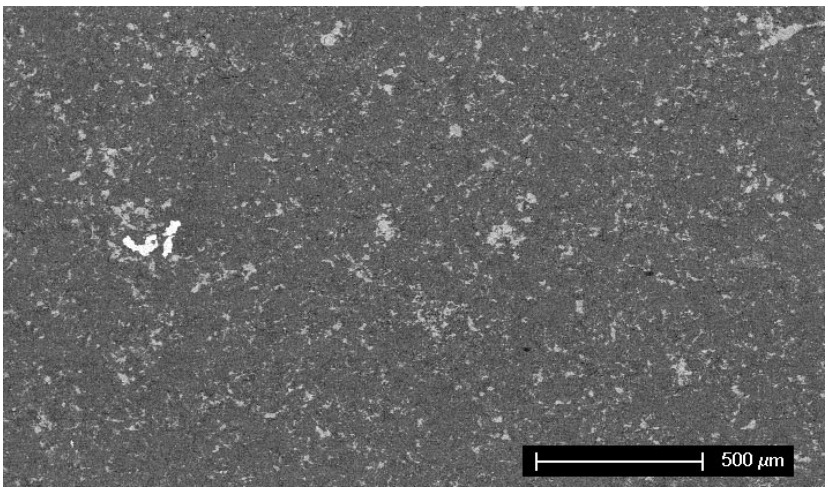

Figure 43. Surface of 0.1 wt.% Y NiCoCrAlY Coating after 100 Cycles at 1100°C

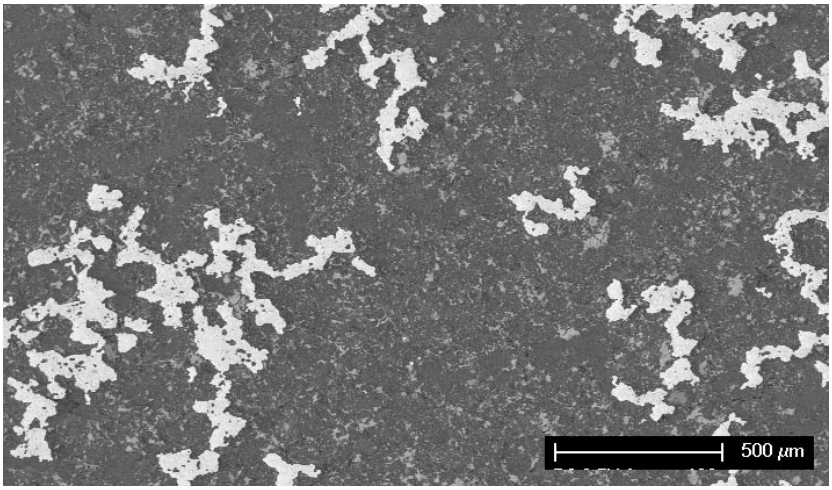

Figure 44. Surface of 0.5 wt.% Y NiCoCrAlY Coating after 100 Cycles at 1100°C

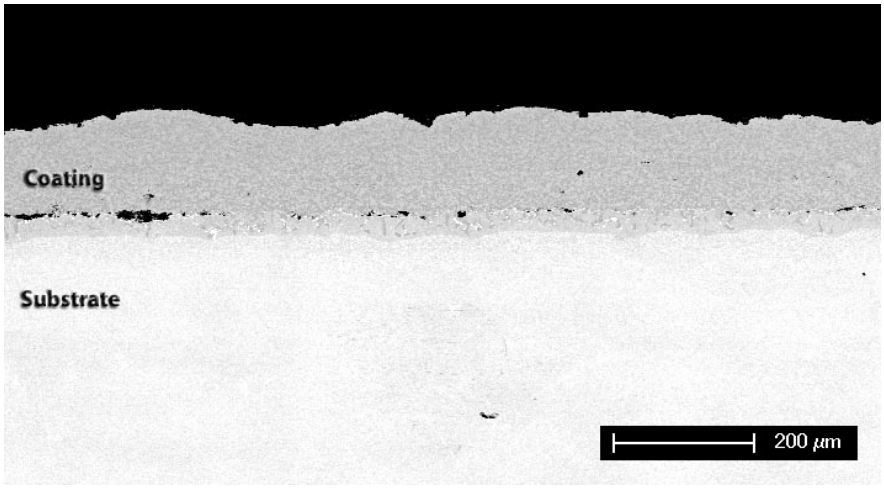

Figure 45. Cross-section of As-Received Coating Containing 0.5 wt.% Y after 100 cycles

Figure 45 shows the cross-section of the sample at relatively low magnification. The overall coating thickness does not appear significantly changed, but the surface has developed a slightly wavy appearance and several small protrusions can be seen at the coating surface. One of these protrusions is shown at higher magnification below. In both Figures, 46 and 47, the thermally grown alumina layer is clearly present and appears to be 4-5 μm thick. The slight separation between the coating surface and the oxide layer is most likely a result of the metallographic preparation. Figure 47 shows the protrusion at still higher magnification and particles containing yttrium can be seen both around the protrusion and incorporated into the oxide itself. At this point, the protrusion is only extending a little more than 5 μm into the coating, but would be expected to grow were the sample put back into test. This attack is obviously undesirable, as eventually the protrusion may extend through the whole thickness of the coating, at which time the protective effect on the substrate would be lost.

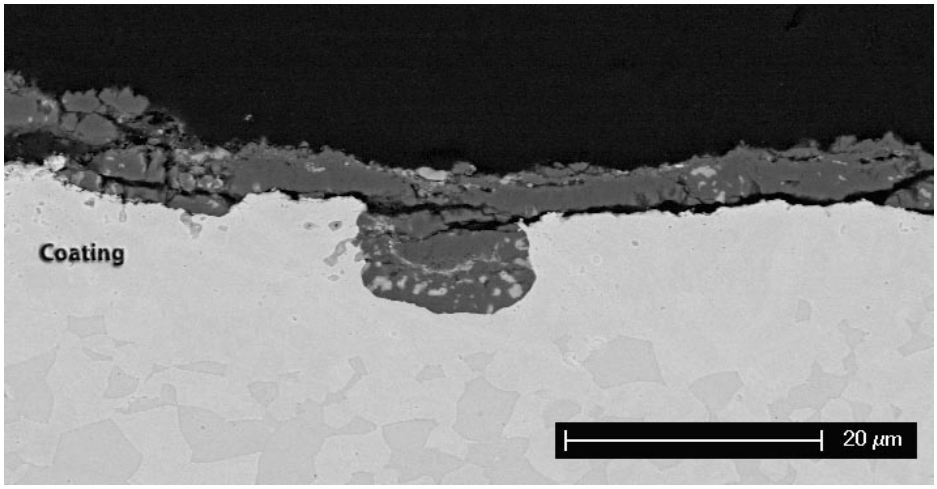

Figure 46. Oxide-filled Protrusion in As-Received Coating

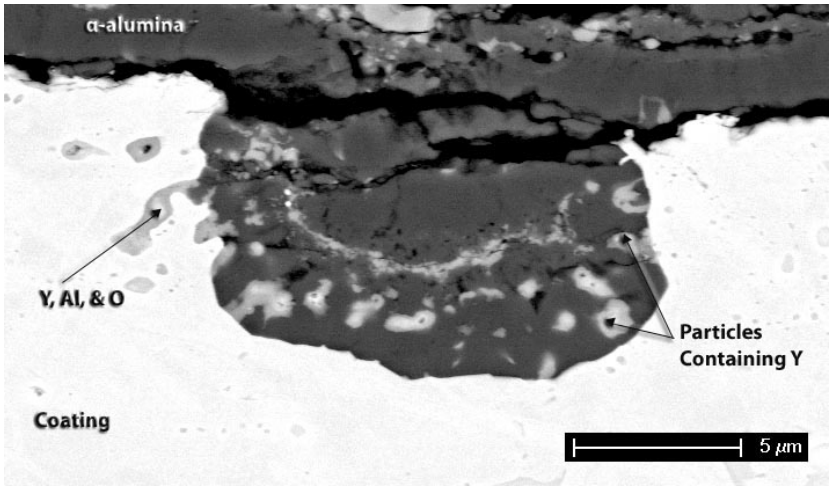

Figure 47. Yttrium Particles in As-Received Coating

After 300 cycles at 1100°C, another sample containing 0.5 wt.% Y was removed and cross-sectioned. This sample had been light grit blasted prior to exposure. Figure 48 shows the cross-sectional image of the sample. The surface looks fairly irregular and several protrusions can be seen extending into the coating. Higher magnification of one of the protrusions is shown in Figure 49. The darker β-phase is still present in large quantities, but has been depleted near the coating-TGO interface.

Figure 49 shows quite clearly that yttrides are present around the protrusion and in the oxide that remains at the tip of the protrusion. This was seen in the areas surrounding all of the protrusions in this sample. This protrusion extends more than 10 μm into the coating, making it twice as deep as that observed in the as-received sample after 100 cycles.

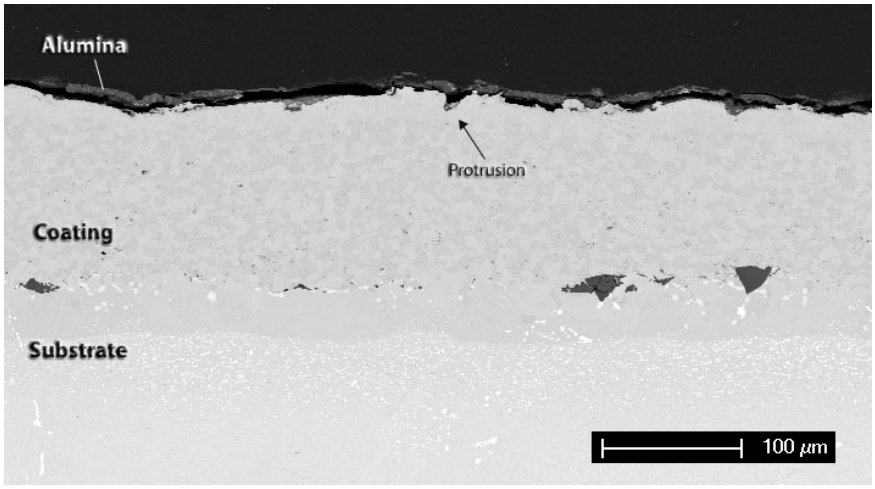

Figure 48. 0.5 wt.% Y, LGB Coating after 300 Cycles

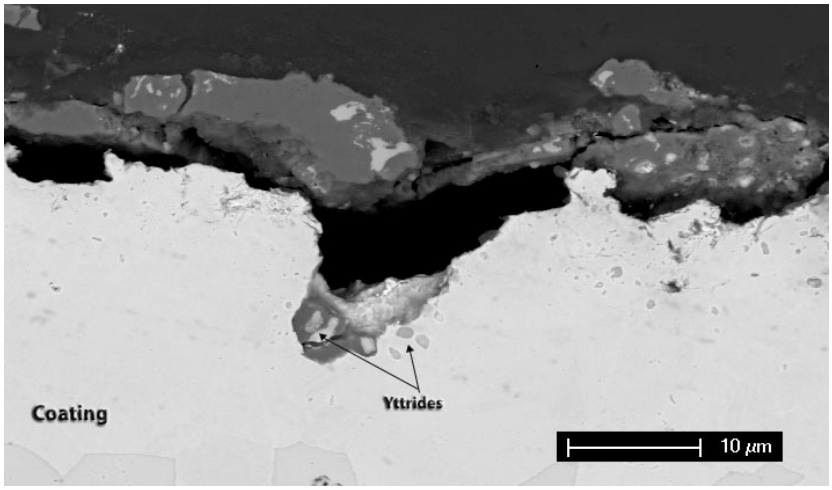

Figure 49. Protrusion in Coating after 300 Cycles

After 400 cycles, an as-received sample containing 0.1 wt.% Y was removed from the furnace and examined. The cross-section of the sample is shown in Figure 50.

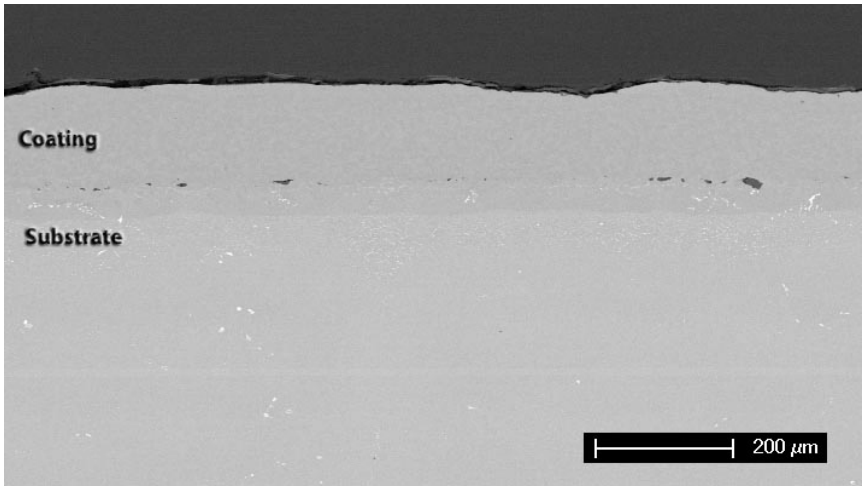

Figure 50. 0.1 wt.% Y, As-Received Coating after 400 Cycles

The surface has a slightly wavy appearance, but no protrusions are evident at the surface of the coating. This is compared to the as-received sample containing 0.5 wt.% Y that exhibited protrusion formation after only 100 cycles.

The next two samples were removed after 1000 cycles at 1100°C. Both samples were light grit blasted and one contained 0.1 wt.% Y and the other contained 0.5 wt.% Y. In Figure 51, there is still a large amount of the β-phase clearly visible. It is also possible to see the region just under the coating/TGO interface where the β-phase has been depleted as the TGO formed. The coating is not perfectly smooth and has several small notches in the surface, but it does not contain any deep protrusions. One of the small oxide filled protrusions can be seen at higher

magnification in Figure 52. As with most of the protrusions observed in these samples, yttrium rich particles were found in the coating adjacent to the protrusion. This protrusion is roughly ten microns deep and the TGO on the coating surface is about five microns thick.

Figure 53 shows the sample containing 0.5 wt.%Y after 1000 cycles. This sample was etched to better illustrate the β-phase. Comparing this figure to Figure 51, it can be seen that much more β-phase remained in the 0.1 wt.% sample than in the 0.5 wt.% sample. This sample had several small protrusions beginning to form, one of which is shown in Figures 54 and 55.

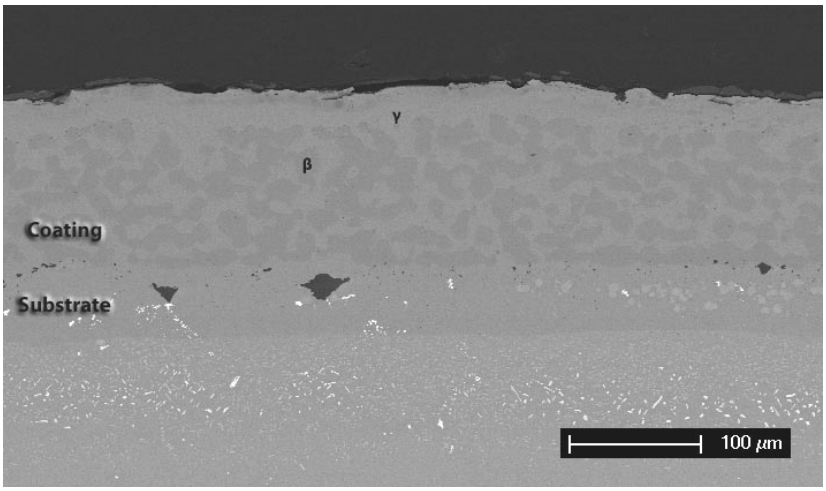

Figure 51. LGB Sample with 0.1 wt.% Y after 1000 Cycles

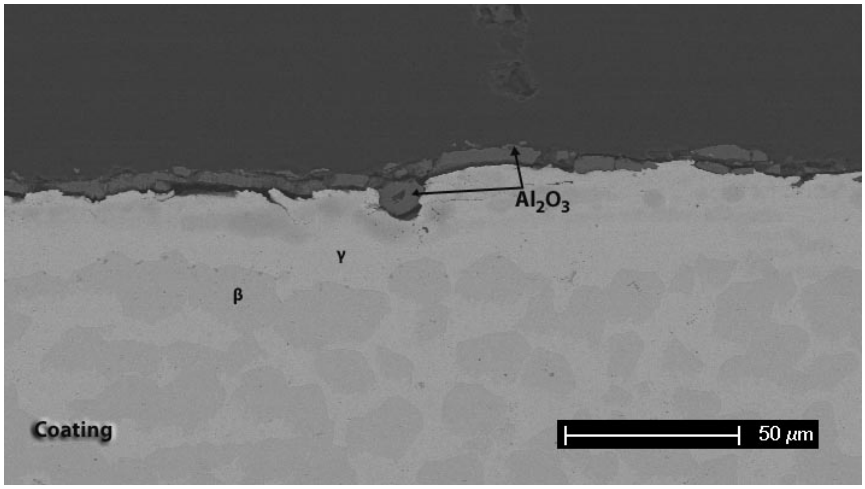

Figure 52. Small Protrusion in 0.1 wt.% Y, LGB Sample after 1000 Cycles

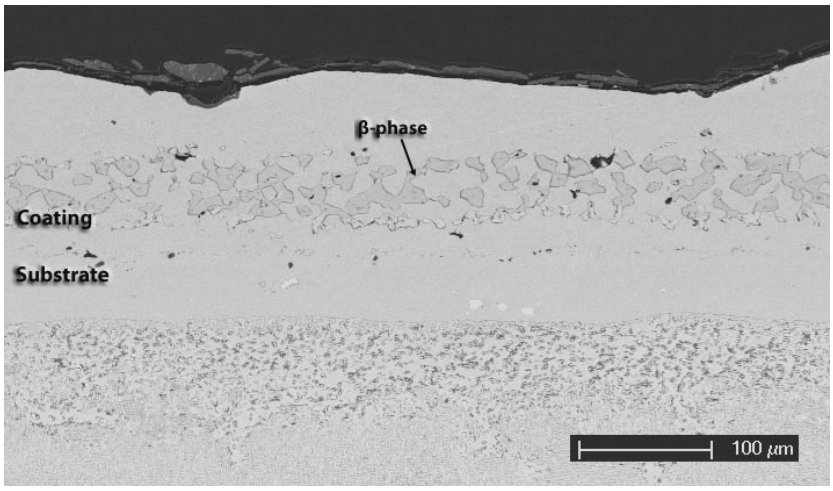

Figure 53. LGB Sample with 0.5 wt.% Y after 1000 Cycles

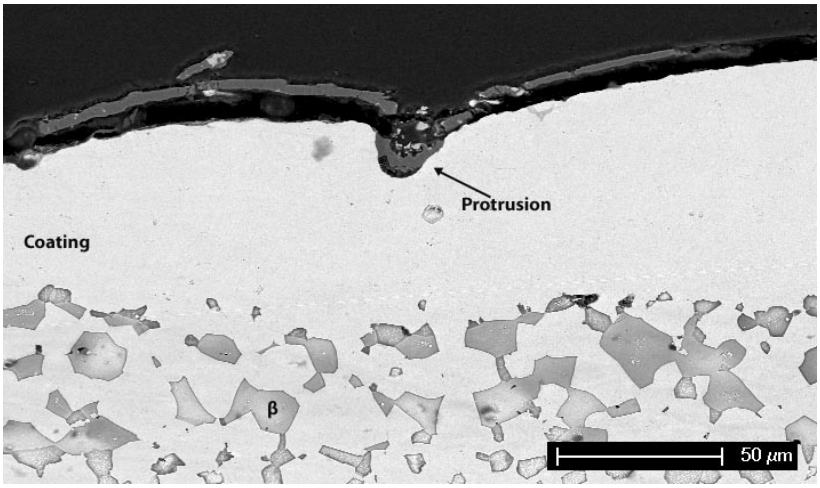

Figure 54. Protrusion in 0.5 wt.% Y Sample after 1000 Cycles

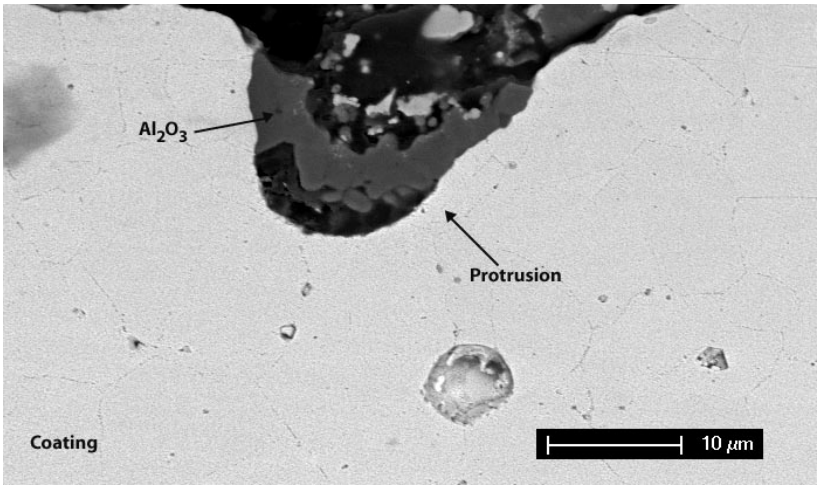

Figure 55. Protrusion and Grain Boundaries in Coating after 1000 Cycles

The protrusion is 20-30 microns deep and filled with alumina. In Figure 55, it is possible to faintly see the grain boundaries in the coating in the area surrounding the protrusion. The grains appear to be fairly equiaxed and about ten microns in diameter.

As in the initial set of samples, the second group also showed preferential yttrium oxidation resulting in protrusions in the samples with 0.5 wt.% Y that had rough surfaces. These samples never developed the blue oxide that was observed in the original batch. No cracking was observed in these samples and none of the protrusions had propagated completely through the coating after 1000 cycles at 1100°C.

The differences in the specimen geometry between the first and second batch of samples may result in different stresses being generated in the coatings. This may explain why the blue oxide was observed in the first round of tests, but not the second as well as why the protrusions did not appear to have propagated through the coatings in the second experiment. It has been hypothesized that to get the deep protrusions seen in the first batch of samples, protrusion

development and cracking are needed. While protrusion development was observed in the second batch of samples containing 0.5 wt.% Y, there was no evidence of cracking.

5.1.2 Cyclic Oxidation of Platinum Aluminide Coatings

Platinum-modified aluminide coatings were also tested cyclically at 1100°C in laboratory air as a comparison to the NiCoCrAlY coatings. A plot of weight change versus time for the samples is shown in Figure 56. All of the samples followed nearly the same pattern of weight gain and loss. Initially, the samples gained mass as they began to oxidize. This continued until they had undergone 1000 cycles, at which time the samples began a continuous, gradual weight loss.

Figure 57 shows a cross-section of a PtAl coating in the as-received condition with no exposure. The coating appears to be slightly more than 50 microns thick. The wavy appearance of the surface of the coatings is due to the presence of grain boundary ridges. These occur due to faster outward diffusion through the grain boundaries than in the surrounding areas.

The shortest oxidation time at which a PtAl coating was examined was 1000 cycles. Micrographs of this sample are shown in Figures 58 to 60. After just 1000 cycles, the surface has become highly irregular. There are no protrusions as were seen in the NiCoCrAlY's.

Figure 60 shows the coating at higher magnification. This sample has been etched to better show the microstructure. In this image, it is seen that large voids have formed at the coating substrate interface and one of the voids has connected to the surface of the coating. At this point the coating would no longer be protective. Since this occurred after relatively short time, it is possible that it may be due to a defect in this particular coating.

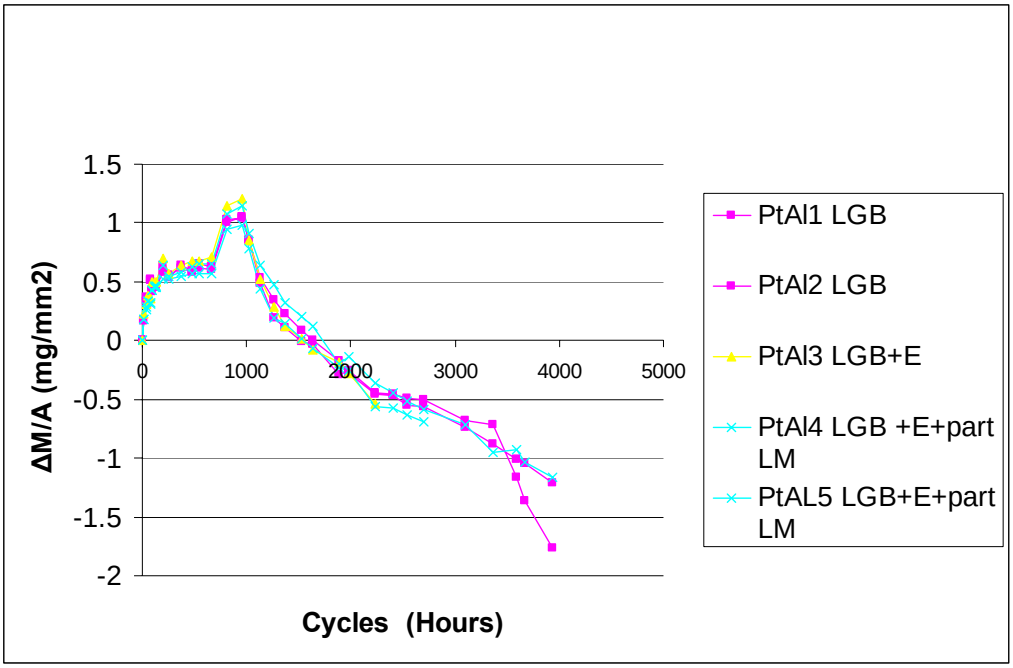

Figure 56. Weight Change vs. Time Plot for PtAl Cyclic Oxidation

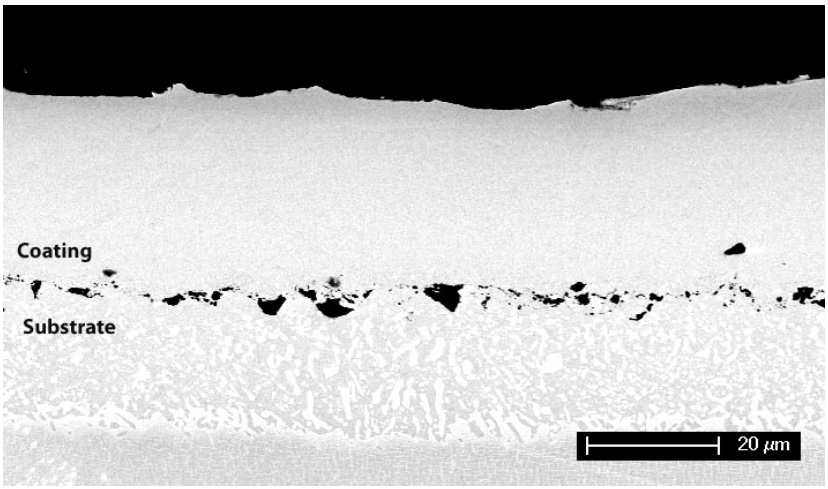

Figure 57. Cross-section of As-Received PtAl Coating

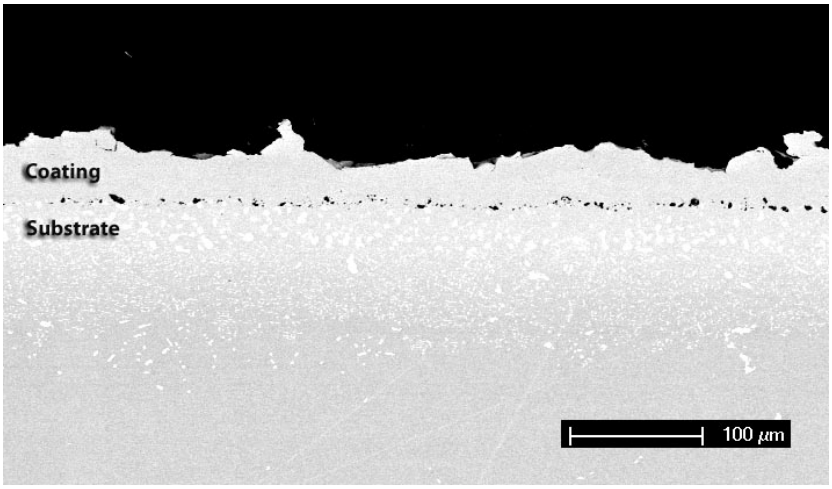

Figure 58. LGB PtAl Coating after 1000 Cycles at 1100°C

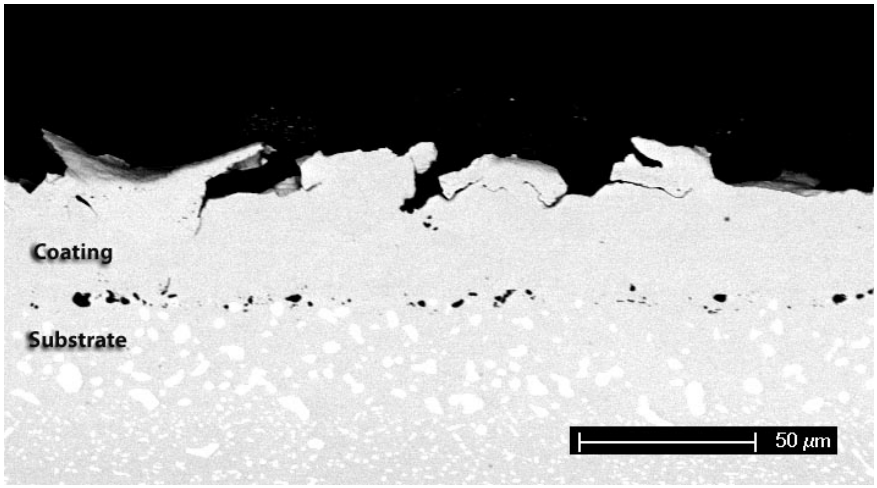

Figure 59. Irregular Surface of PtAl after 1000 Cycles

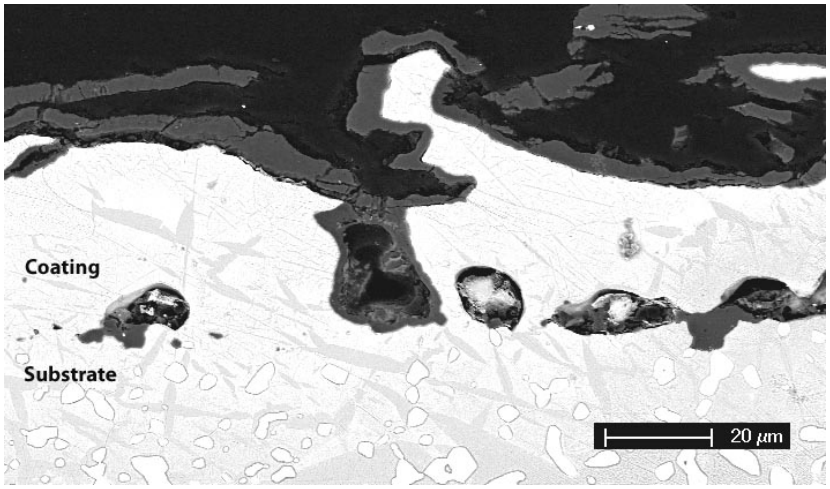

Figure 60. Void Formation in PtAl Coating after 1000 Cycles

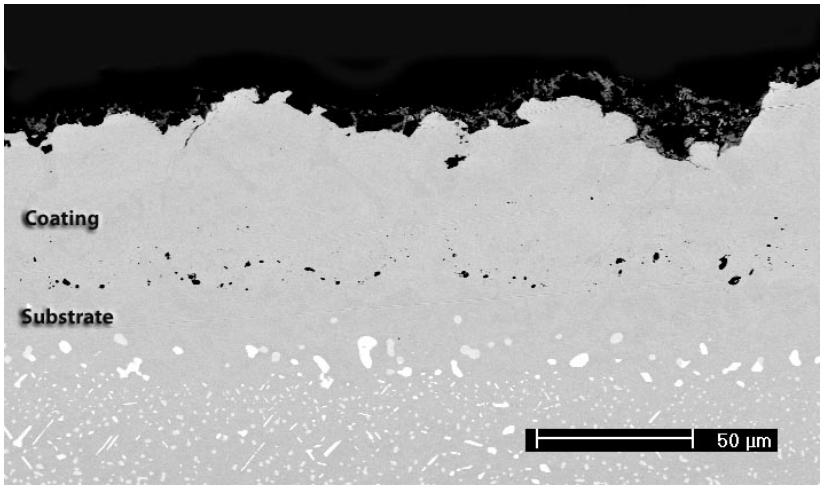

Figure 61. LGB & Etched PtAl Coating after 2300 Cycles at 1100°C

Another sample was removed after 2300 cycles. This sample had been light grit blasted and etched to remove the grit blast particles. In Figure 61, it is observed that this sample looks better than the sample exposed for 1000 cycles. The surface is irregular, but there are no large voids forming at this time at the coating/substrate interface.

Figure 62 shows a low magnification image of a PtAl coating that was also light grit blasted and etched. This sample had been exposed for 2,850 cycles. The surface of the coating appears very irregular and the coating is very thin in some areas. This is seen more easily in Figure 63 at higher magnification.

The longest time at which a PtAl was examined in this study was 4500 cycles. Images of this sample are shown in Figures 64 to 66. At low magnification, it is easy to see that large voids have formed along the entire length of the coating/substrate interface. At this point, the coating is only around 25 microns thick.

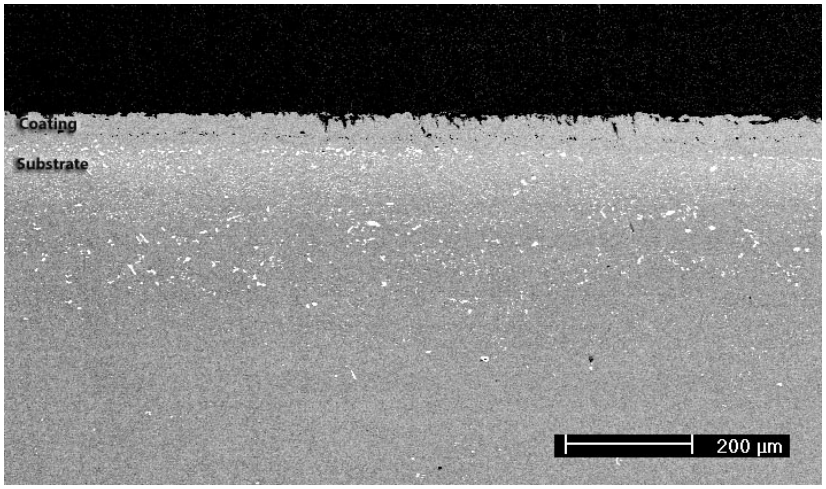

Figure 62. LGB & Etched PtAl Coating after 2850 Cycles at 1100°C

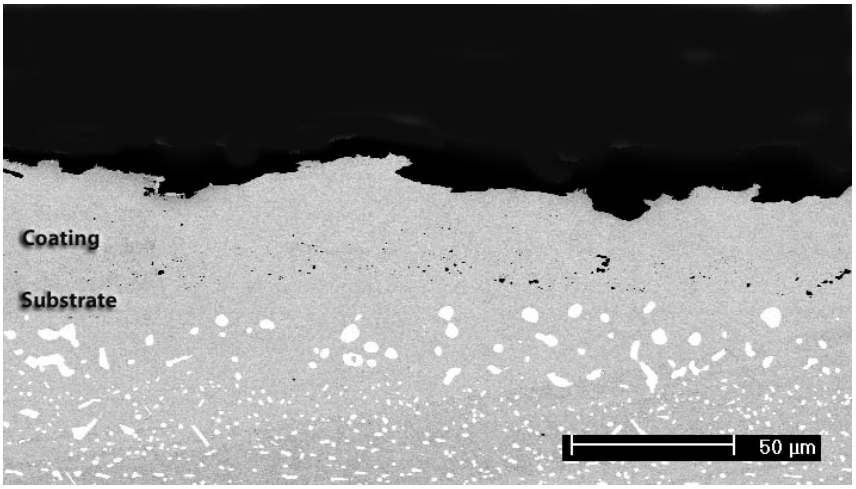

Figure 63. PtAl Coating Degradation after 2850 Cycles

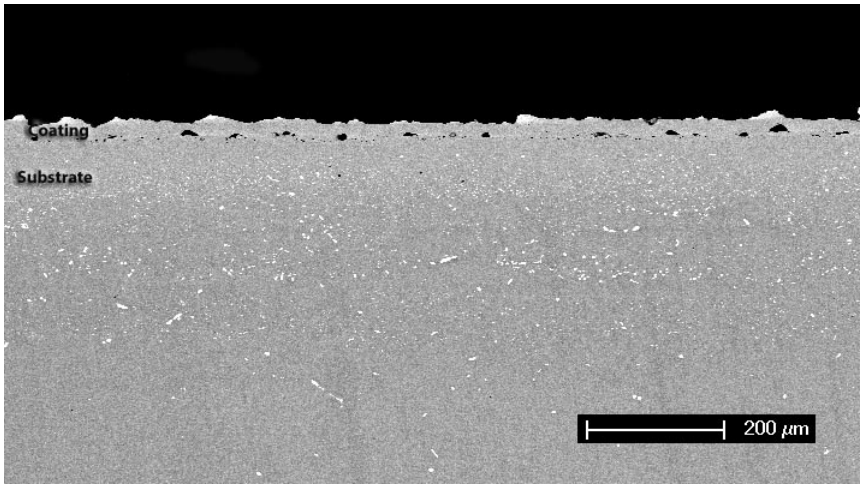

Figure 64. LGB and Etched PtAl Coating after 4500 Cycles at 1100°C

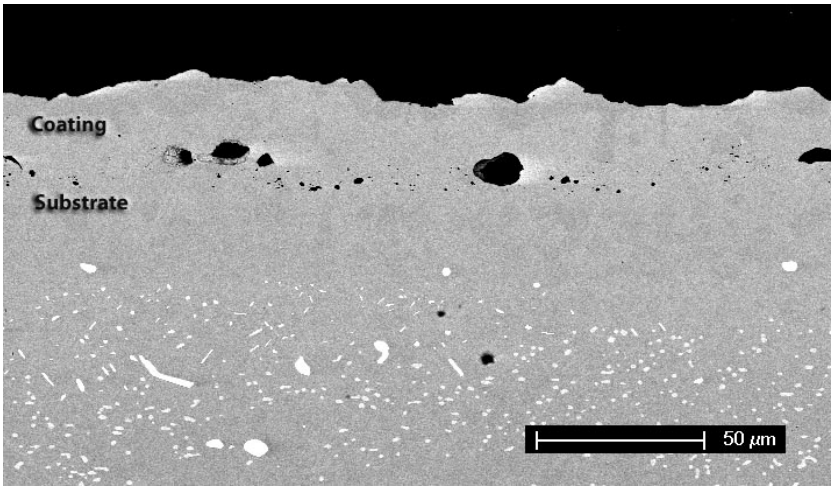

Figure 65. Voids at Coating/Substrate Interface after 4500 Cycles

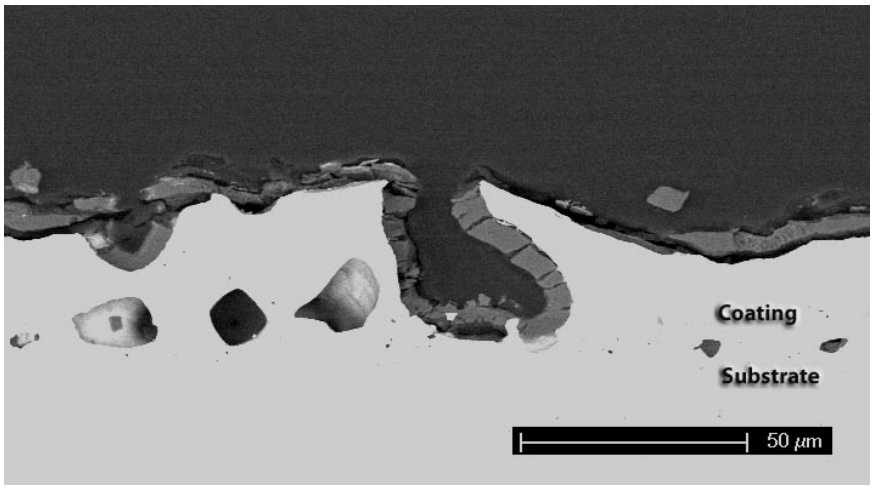

Figure 66. Failure of PtAl Coating after 4500 Cycles

Figure 66 shows a large void that has connected to the surface of the coating. After the void broke through the surface, a layer of alumina grew and coated the inner surface of the void. Other large voids are seen on the left side of the image.

In conclusion, regardless of surface condition, the PtAl coatings had similar behavior and mass change. When the coatings were examined after 1000 cycles, the surface was already very irregular and voids had begun to form at the coating/substrate interface. It can then be proposed that failure in these coatings results from a thinning of coating at long exposure times, which subsequently makes it easier for large voids, formed at the coating/substrate interface by interdiffusional processes, to connect to the coating surface causing failure. Although the exact mechanism of void formation is not understood, these results agree with those observed by Yanar, Pettit and Meier in previous studies of this topic [1]. It is possible that small voids are present in the as-processed coatings and that they grow by a vacancy condensation mechanism as aluminum diffuses into the substrate and to the coating surface during exposure.

5.1.3 Comparison of Coatings for Cyclic Oxidation Resistance

Comparing the two types of coatings, NiCoCrAlY and PtAl, leads to several conclusions. The rough NiCoCrAlY coatings containing 0.5 wt.%Y showed very early signs of degrading and oxidation by the appearance of the blue oxide. When these samples were cross-sectioned, it was seen that they failed by the formation of large oxide protrusions that penetrated the entire coating. The hand polished NiCoCrAlY's with 0.5 wt.%Y and all of those with 0.1 wt.% Y did not develop protrusions and, in fact, did not fail at all during the length of the test.

In comparison, the PtAl coatings appear to fail by formation of voids at the coating/substrate interface that grow until the coating surface has been penetrated. This is somewhat opposite to how the NiCoCrAlY's fail. This failure began in the PtAl's after only 1000 cycles.

From these results, it has been found that the lifetimes of the PtAl coatings are comparable to those of the 0.5 wt.% Y coatings with rough surfaces failing after a few thousand cycles. Both the fine polished 0.5 wt.%Y and all of the 0.1 wt.% Y NiCoCrAlY coatings exhibited significantly longer lifetimes in excess of 6500 cycles at 1100°C.

The impressive performance of the NiCoCrAlY coatings with 0.1 wt.% Y, and the polished NiCoCrAlY with 0.5 wt.%Y are due to the lack of protrusion development in these coatings. The yttrium improves the oxide scale adherence, but does not participate in the oxide scale development. The platinum aluminide coatings were thin (30-40μm) compared to the NiCoCrAlY coatings (~140 μm). Thicker platinum aluminide coatings may give longer lives than those observed in this investigation, but the failure mechanism would probably be the same.

5.1.4 Future Work

Future studies should include an examination of the role that sample geometry plays in the failure of the NiCoCrAlY coatings. Comparisons of the stresses that develop in round, disk-shaped specimens as opposed to the smaller rectangular coupons should be performed. These findings can be used to determine whether the absence of the blue oxide spinel and cracking on the second batch of samples was due to specimen geometry or other factors. Isothermal tests will also be performed on these samples.

Tests will be continued on the 0.1 wt.%Y NiCoCrAlY coatings that remain. They will continue to be cycled until they exhibit symptoms of failure at which time they can be examined and, hopefully, the characteristics that allowed them to have such long lifetimes can be determined and replicated.

6.0 CONCLUSIONS

In conclusion, NiCoCrAlY coatings with either 0.1 weight percent yttrium or 0.5 weight percent yttrium as well as platinum modified aluminide coatings were studied to determine their resistance to cyclic oxidation conditions. The samples were exposed at 1100°C in a bottom-loading furnace in laboratory air. Samples were examined and characterized using optical and scanning electron microscopy. The coatings were subjected to various surface treatments prior to their exposure. Samples were either exposed as-received, with no modification, light grit blasted, light grit blasted and etched with NaOH to remove grit particles, or hand polished.

The NiCoCrAlY samples containing 0.5 wt.% Y in the as received, LGB and LGB and etched condition failed after the formation of large oxide protrusions caused by cracking in the coating in concave regions of the coating where yttrium had been preferentially oxidized. The hand polished NiCoCrAlY coatings containing 0.5 wt.%Y did not develop any protrusions and did not fail in the time they were left in test. Protrusions were not observed on any of the 0.1 wt.%Y NiCoCrAlY coatings regardless of their surface treatment. No coating containing 0.1 wt.%Y failed in test, even after 6500 cycles. The PtAl coatings all failed by the same mechanism independent of the surface treatment. This occurred by void formation at the coating/substrate interface that eventually reached the coating surface.

It was concluded that, in the NiCoCrAlY system, the roughness of the coating surface as well as the amount of yttrium present to oxidize in the coating plays a large role in the

coating lifetime. In the rough 0.5 wt.%Y NiCoCrAlY's, the yttrium accumulated in the concave regions causing preferential oxidation. By polishing the surface of these samples, the concave regions were eliminated and protrusions did not form. It is believed that 0.1 wt.%Y is not a sufficient amount to allow for protrusion formation. In the PtAl coatings, surface preparation did not appear to have any effect on the coating lifetime. The PtAl coatings and the un-polished, 0.5 wt.%Y NiCoCrAlY coatings exhibited similar lifetimes of a few thousand cycles. The polished 0.5 wt.%Y NiCoCrAlY coating and all of the 0.1 wt.%Y coatings showed much improved lifetimes, with failure not being reached in the time allowed.

BIBLIOGRAPHY

1. Yanar, N.M., Pettit, F.S., Meier, G.H, *Failure Characteristics during Cyclic Oxidation of Yttria Stabilized Zirconia Thermal Barrier Coatings Deposited via Electron Beam Physical Vapor Deposition on Platinum Aluminide and on NiCoCrAlY Bond Coats with Processing Modifications for Improved Performances.* Metallurgical and Materials Transactions, 2006. **37A**: p. 1563-1580.

2. Mumm, D.R., Evans, A.G., Acta. Mater., 2000. **48**: p. 1815.

3. Gil, A., Shemet, V., Vassen, R., Subanovic, M., Toscano, J., Naumenko, D., Singheiser, L., Quaddakers, W., *Effect of surface condition on the oxidation behaviour of MCrAlY coatings.* Surface Coatings and Technology, 2006. **201**: p. 3824-3828.

4. Birks, N., Meier, G. H., Pettit, F. S., *Introduction to the High-Temperature Oxidation of Metals, 2nd Edition*. 2006, New York: Cambridge University Press.

5. Wang, H.A., Kroger, F.A., *Chemical Diffusion in Polycrystalline Al_2O_3.* J. Amer. Cer. Soc., 1980. **63**: p. 613.

6. Alkebro, J., Begin-Colin, S., Mocellin, A., Warren, R., , Journal of European Ceramic Society, 2000. **20**: p. 2169.

7. Shen, Z.E., Å, Nygren, M., *Oxide /oxide composites in the system Cr_2O_3-Y_2O_3-Al_2O_3.* J. of European Ceramic Society, 2000. **20**: p. 625-630.

8. Parthasarathy, T.A., Mah, T., Keller, K., *Creep Mechanism of Polycrystalline Yttrium Aluminum Garnet.* J. Amer. Cer. Soc., 1992. **75**(7): p. 1756-1759.

9. Smith, J.S., Boone, D.H., , *Platinum Modified Aluminides – Present Status*, in *Gas Turbine and Aeroengine Congress*. 1990, ASME: New York.

10. Stern, K.H., ed. *Metallurgical and Ceramic Protective Coatings*. 1996, Chapman & Hall: London.

11. Schaeffer, J., Kim, G.M., Meier, G.H., Pettit, F.S., *The effects of precious metals on the oxidation and hot corrosion of coatings*, in *The Role of Active Elements in the Oxidation Behavior of High Temperature Metals and Alloys*, E. Lang, Editor. 1989, Elsevier: Amsterdam. p. 231.

12. Giggins, C.S., Pettit, F.S., *Oxidation of Ni-Cr-Al Alloys Between 1000 and 1200 C* J. Electrochem. Soc., 1971. **118**: p. 1782-1790.

13. Griffiths, W.T., Pfeil, L.B. 1937: U.K.

14. Whittle, D.P., Stringer, J., *Improvement in High Temperature Oxidation Resistance by Additions of Reactive Elements or Oxide Dispersions.* Phil. Trans. R. Soc. Lond., 1980. **A295**: p. 309-329.

15. Hou, P.Y., Stringer, J., *Effect of reactive element additions on the selective oxidation, growth and adhesion of chromia scales.* Mater. Sci. Eng., 1995. **A202**: p. 1-10.

16. Ashary, A., *Adherence of $A1_20_3$ scales on MCrA1 type coating alloys*, in *Department of Metallurgical Engineering*. 1985, University of Pittsburgh.

17. Francis, J.M., Whitlow, W.H., *Improvements in High Temperature Oxidation Resistance by Additions of Reactive Elements or Oxide Dispersions.* Corros. Sci. , 1965. **5**: p. 701-710.

18. Wood, G.C., Boustead, J., *The Influence of Group IIIA Metals on the Oxidation of Iron-Chromium Alloys* Corros. Sci., 1968. **8**: p. 719-723.

19. Nanni, P., Stoddart, C.T.H., Handros, E.D., Mater. Chem., 1976. **1**: p. 297-320.

20. Golightly, F.A., Scott, F.H., Wood, G.C., Oxid. Met. , 1976. **10**: p. 163-187.

21. Christensen, R.J., Tolpygo, V.K., Clarke, D.R., *The Influence of the Reactive Element Yttrium on the Stress in Alumina Scales Formed by Oxidation.* Acta Mater., 1997. **45**(4): p. 1761-1766.

22. Tien, J.K., Pettit, F.S., *Mechanism of Oxide Adherence on Fe-25Cr-4Al (Y or Sc) Alloys.* Metallurgical Transactions 1972. **3**: p. 1587-1599.

23. Kuenzly, J.D., Douglas, D.L., *Oxidation Mechanism of Ni_3Al Containing Yttrium.* Oxid. Met., 1974. **8**: p. 139-178.

24. Allam, I.A., Whittle, D.P., Stringer, J., *Oxidation Behavior of CoCrAl Systems Containing Active Element Additions.* Oxid. Met., 1978a. **12**: p. 34-67.

25. Pfeiffer, H., Werkstoffe Korros., Mannheim 1957. **8**: p. 574-579.

26. Funkenbusch, A.W., Smeggil, J.G., Bornstein, N.S., *Reactive Element-Sulfur Interaction and Oxide Scale Adherence.* Met. Trans., 1985. **16A**: p. 1164-1166.

27. Smeggil, J.G., Funkenbusch, A.W., Bornstein, N.S., *A Relationship between Indigenous Impurity Elements and Protective Oxide Scale Adherence Characteristics.* Met. Trans., 1986. **17A**: p. 923-932.

28. Tolpygo, V.K., Clarke, D.R., Murphy, K.S., *The Effect of Grit Blasting on the Oxidation Behavior of a Platinum-Modified Nickel-Aluminide Coating.* Met. Trans., 2001. **32A**: p. 1467-1478.

29. Haynes, J., *Potential influences of bond coat impurities and void growth on premature failure of EB-PVD TBCs.* Scripta mater., 2001. **44**: p. 1147-1152.

30. Taylor, T.A., Walsh, P.N., *Thermal expansion of MCrAlY alloys.* Surface Coatings and Technology, 2004. **24**: p. 177-178.

31. Haynes, J.A., Pint, B.A., Porter, W.D., Wright, I.G., *Comparison of Thermal Expansion and Oxidation Behavior of Various High-Temperature Coating Materials and Superalloys.* Mater. at High Temp., 2004. **87**: p. 21.